GNGTS 2024

SEISMICITY, VOLCANOES, DATA AND MODELS

Session 1.3

Physical models for the Solid Earth and integration between modeling and data of different nature

Convenors of the session:
Anna Maria Marotta (UniMI) – anna.maria.marotta@unimi.it
Carla Braitenberg (UniTS) – berg@units.it
Barbara Orecchio (UniME) – barbara.orecchio@unime.it

Contributions recommended for this session:

- **Forward and inverse physical models of Solid Earth processes at different wavelengths and time scales**
  - **Surface tectonic deformation**
  - **Post glacial rebound**
  - **Mantle dynamics**
  - **Relative Sea level change**
  - **Earthquakes and the internal structure of the Earth**
- **Techniques and quantitative methods for analyzing large amounts of geophysical data of different nature and at very high resolution, both terrestrial and satellite (eg. GNSS, SAR, Gravitational, Seismological, Magnetometric, thermal)**
  - **Rheological characterization of the crust and mantle**
  - **Numerical models of geomagnetic anomalies**
  - **Shape and size of the Earth**
  - **Earth's gravitational field**
  - **Numerical modeling of Gravimetric Anomalies**
  - **Observation of the Earth from Space – GNSS, InSAR**
  - **Surface geodetic deformation**
- **Integrated analyses between physical modeling and data (natural, experimental and observational from satellite)**
- **Interactions between Solid Earth processes and the Hydrosphere and the Atmosphere**
- **Planetology studies regarding the internal physical processes occurring on planets, both internal and external to the solar system, are also welcome**

On opposite sides of Naples: an intriguing contemporaneous onset of deep deflation below Vesuvio and the ongoing Campi Flegrei uplift.

A. Amoruso[1], L. Crescentini[1]

[1] Department of Physics, University of Salerno, Fisciano, Italy

Campi Flegrei and Vesuvio volcanoes are located on opposite sides of Naples and it is of great interest to get clues of possible mutual interactions or coincidences in their recent deformation dynamics.

As for Campi Flegrei, after the large uplift occurred at the beginning of the 80s and the general subsidence from 1985 to 2001, since the early 2000s it is uplifting mostly at an accelerating rate and its dynamics is probably driven by deep magma inflation (Amoruso and Crescentini, 2022).

As for Vesuvio, we analysed the ground displacement time series in the whole Vesuvian area and its surroundings around the early 2000s, using 1993–2010 ERS/ENVISAT ascending- and descending-orbit line-of-sight displacements. Our computations show a sudden trend change around 2001: pre-2001 velocity maps indicate subsidence mainly occurring inside the caldera rim and in a few spots around 10 km from the summital crater, thus confirming previously published results by others; post-2002 velocity maps provide evidence of general subsidence in the whole Vesuvian area. This last arrangement of the ground displacement field is made even clearer by subtracting the post-2002 velocity from the pre-2001 one and is consistent with the deflation of a deep pressurised source and the decrease of Vesuvio's deep seismicity at the beginning of 2002. (Amoruso and Crescentini, 2023)

The reveal of the coincidence between the transition from deflation to inflation at Campi Flegrei and the onset of deflation below Vesuvio may suggest the possible transfer of magma and/or magmatic fluids and the influence of the dynamics of one plumbing system on the other.

Reference

Amoruso A. and Crescentini L.; 2022: Clues of Ongoing Deep Magma Inflation at Campi Flegrei Caldera (Italy) from Empirical Orthogonal Function Analysis of SAR Data. Remote Sens., 14, 5698, DOI 10.3390/rs14225698.

Amoruso A. and Crescentini L.; 2023: DInSAR Data Reveal an Intriguing Contemporaneous Onset of Deep Deflation below Vesuvio and the Ongoing Campi Flegrei Uplift. Remote Sens. 2023, 15, 3038. DOI 10.3390/rs15123038.

Corresponding author: aamoruso@unisa.it

Monitoring the Tonga volcano starting from the unrest of 2014/2015 to the 2021/2022 explosion with Sentinels

C. Braitenberg

Department of Mathematics, Informatics and Geosciences (MIGe), University of Trieste, Trieste, Italy,

This study explores the dynamic evolution of the Tonga volcano, Tonga, throughout its volcanic cycle, with a particular focus on the formation and subsequent disappearance of a new island between Hunga Tonga (HT) and Hunga Ha'Apai (HH) between 2014 and 2023. The island first increased its surface extension in 2015 and vanished in January 2022, by a significant eruption, characterized by a 50 km high ash plume and Tsunami. Leveraging remote sensing techniques, specifically multispectral imaging from the satellite missions Sentinel 2 and SAR imaging from Sentinel 1, the research employs a supervised Random Forest classification algorithm to track the changing subaerial surface area of the volcano. This approach enables the documentation of size variations in the islands, especially during weeks surrounding volcanic unrests. The classifier, trained on nearly cloud-free multispectral images, automatically defines surface area changes over the years. The temporal resolution of area change is constrained by images with less than 5% cloudiness, resulting in 113 Sentinel 2 images between 2016 and 2023, selected from 506 available images. The Sentinel 1 Synthetic Aperture Radar (SAR) images penetrate clouds, and are therefore complementary to the multispectral observations, with the drawback of observing the reflectivity only on up to two bands. Nonetheless the classifier is successful in distinguishing land from ocean, albeit with greater noise. The Sentinel 1 observations start in 2014, extending the time series to cover the volcano unrest of 2014/2015, totalling 213 images. The processing is fulfilled in the Earth Engine cloud computing data facility. Analysis reveals a slight decrease in area change after emplacement of a new island in 2015 and identifies the disappearance of the island bridge connecting HT and HH, along with two smaller islands south of HTHH in 2022. The 2022 unrest is preceded by an increase in island

area weeks before the volcano explosion. The global satellite coverage of the method suggests its potential applicability to automatically detect changes in oceanic areas, distinguishing between water and new volcanic island, thereby providing a means to anticipate upcoming volcanic unrests and document their evolution.

Corresponding author: berg@units.it

Update of the Northern Apennines and Southern Alps velocity field from historical GNSS measurement to the “0 point”.

F. Carnemolla[1], F. Brighenti[2], G. De Guidi[1], A. Di Pietro[2], P. Fabris[3], S. Giuffrida[1], A. Magrin[3], G. Rossi[3], D. Russo[2], L. Tunini[3], D. Zuliani[3].

[1] *Università degli Studi di Catania, Catania, Italy*
[2] *Università degli Studi di Ferrara, Ferrara, Italy*
[3] *Istituto Nazionale di Oceanografia e di Geofisica Sperimentale-OGS, Trieste, Italy*

In the framework of the PRIN 2020 - NASA4SHA Project (Fault segmentation and seismotectonics of active thrust systems: the Northern Apennines and Southern Alps laboratories for new Seismic Hazard Assessments in northern Italy), we have reoccupied 29 points belong to the IGM95 Network focusing on local transects orthogonal to the main compressive structures belong to the Northern Apennines and Southern Alps thrust belts (Fig. 1).

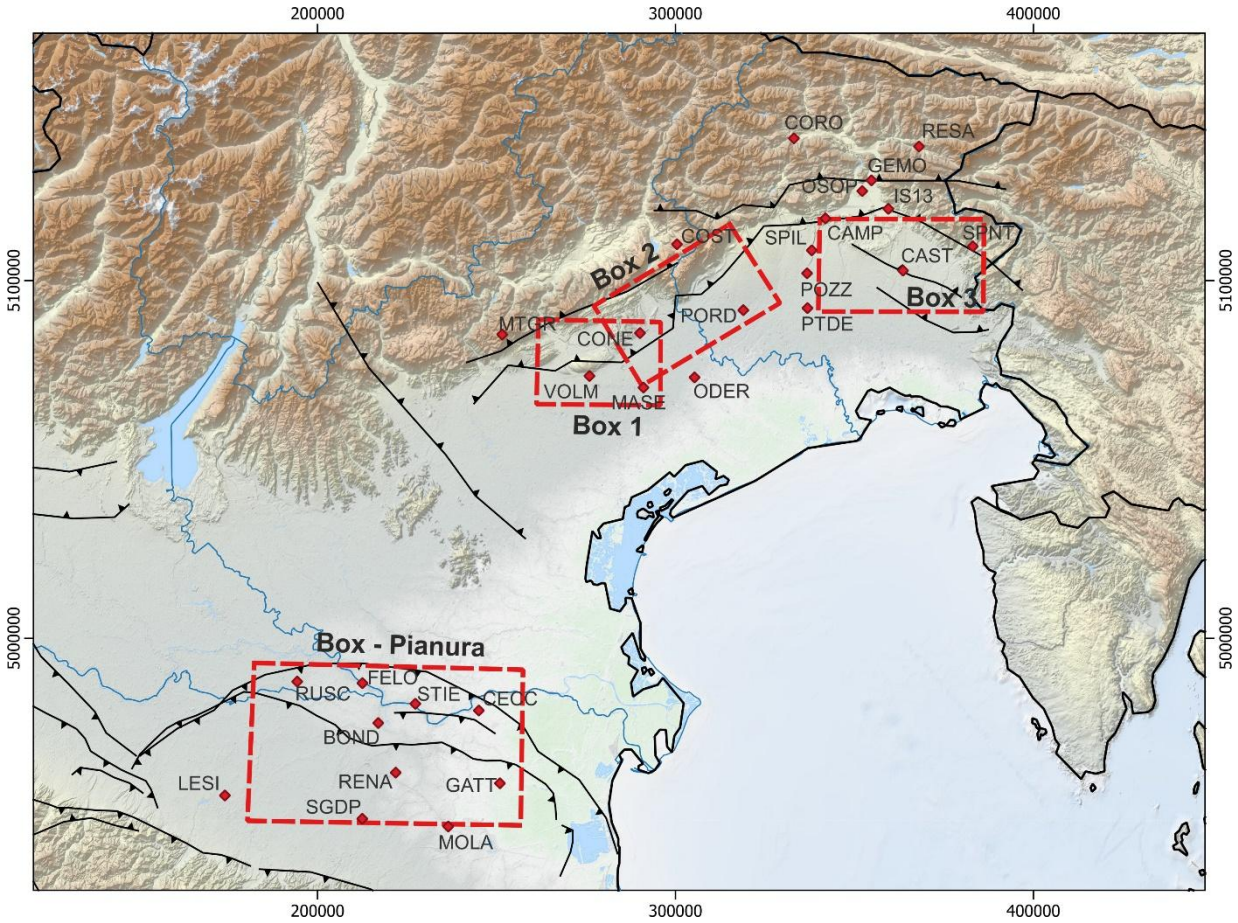

Fig. 1 – IGM95 points reoccupied during the 2023 campaigns

We selected these points, where possible, according to the following criteria:

1. Stability of the monuments;
2. Benchmarks build during the establishment of the IGM95 networks (1993-1995);
3. Number of occupations on the past;

Unfortunately, these criteria are not always respected in particular the second and third criteria, for example eight points (SPNT, PTDE, POZZ, MOLI, IS13, GEMO, CONS and CAMP) were built during the phase of densifications of the network (2000-2001) and four points have only one occupation (VOLM, PTDE, POZZ and MOLI). Moreover we have examined the duration of the measurement session for the old campaign, in particular, the first campaigns (1993) were characterised by an average of 4.5 hours measurement sessions, which decrease to 2 hours in the early 2000's (1996,2000,2006 and 2010).

In addition we have chosen same points close to same continues GPS stations, in order to compare our results to those obtain from the permanent stations.

Obviously, the IGM95 network was created for cartographic and topographic applications, for this reason most of the IGM95 beckmarks do not follow restrictive geodetic requirements for geophysical applications (duration, stability, use of tripod, Anzidei et al. 2008), but, in our opinion, these aspects are probably compensated by their long term velocity (30 years on 2023). However, these IGM95 points were selected in order to improve the strain rate, in term of resolutions, of selected structures on the Northern Apennines and Southern Alps thrust belt, and to establish a "0 points" for the future in order to improve our knowledge about these thrust belt.

The data were processed by Gamit-Globk software using double-difference phase observation with ambiguity resolutions, precise orbits and adopting the absolute phase center model for receiver and satellite antenna. The preliminary velocity field (Fig.2) is expressed in the IRTF14 reference frame with respect to the Eurasian plate (Altamini et al., 2017).

From a preliminary evaluation, the velocity field obtained by IGM95 sites is agree with the compressive dynamics and with that obtained by the permanent stations belong to the RING (Rete Integrata Nazionale GNSS) and FReDNet (Friuli Regional Deformation Network) networks, managed by INGV (Istituto Nazionale di Geofisica e Vulcanologia) and OGS (Istituto Nazionale di Oceanografia e di Geofisica Sperimentale) respectively in the framework of the PRIN2020 - NASA4SHA Project.

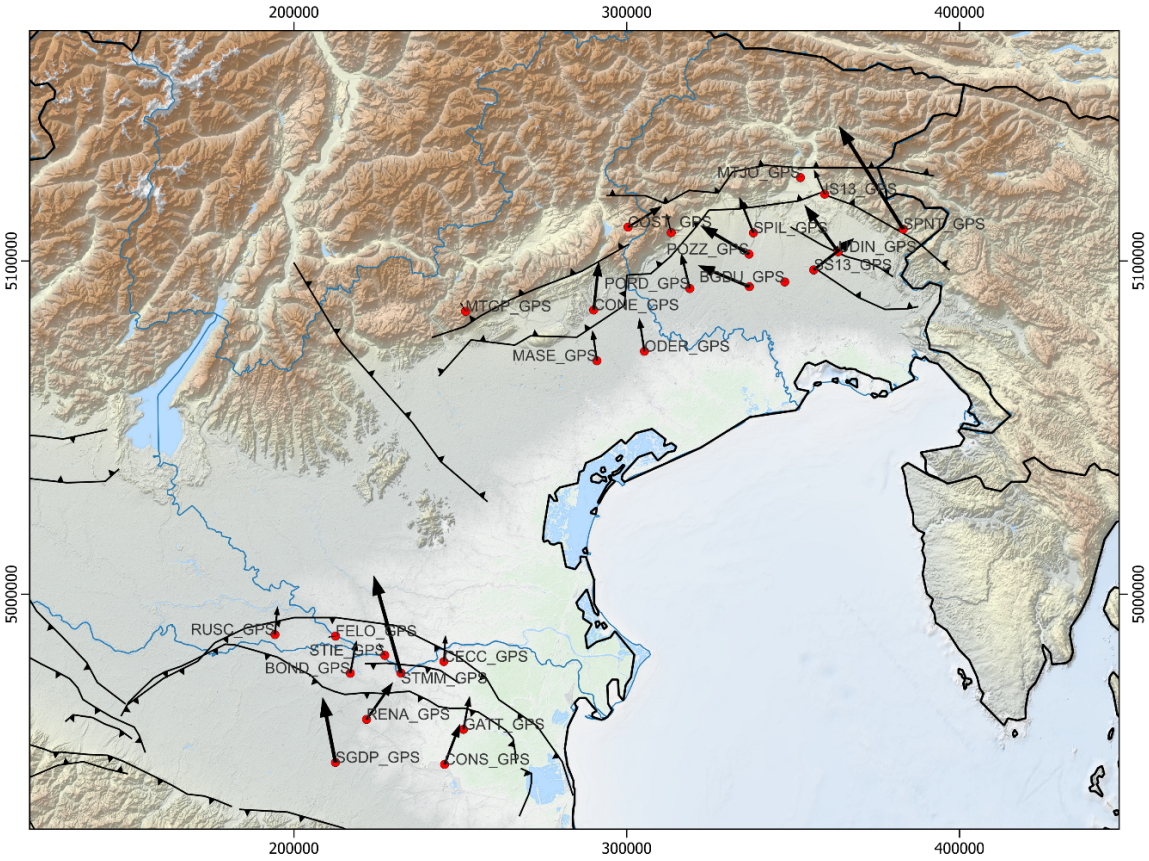

Fig. 2 – Velocity field obtained by IGM95 points.

References

Anzidei M., Baldi P., Serpelloni E.; 2008: The coseismic ground deformations of the 1997 Umbria-Marche earthquakes: a lesson for the development of new GPS networks, Annals of Geophysics, Vol. 51, N. 2/3, April/June 2008.

Altamimi Z., Métivier L., Rebischung P., Rouby H., Collilieux X.; 2017: ITRF2014 plate motion model, Geophys. J. Int., 209, 3, doi:10.1093/gji/ggx136..

Corresponding author: francesco.carnemolla@unict.it

Diffusivity analysis of clustered seismicity in Central-Southern Apennines

G.M. Cipressi[1], A. Vuan[4,5], M.A. Romano[4], G. Lavecchia[2,3], R. de Nardis[2,3]

1 Department of Engineering and Geology, University "G. d' Annunzio" of Chieti-Pescara, Italy

2 DiSPuTer - University of Chieti-Pescara 'G. d'Annunzio', Italy

3 CRUST- Interuniversity Center for 3D Seismotectonics with Territorial Applications, Italy

4 National Institute of Oceanography and Applied Geophysics (OGS), Italy

5 National Institute of Geophysics and Volcanology (INGV), Italy

Seismic swarms are defined as a set of clustered earthquakes with high spatio-temporal variability and with the absence of a main shock. They can originate in different tectonic contexts related to the migration of deep fluids that can alter the stress field (Roland et al., 2009). In particular, the diffusivity parameter, defined by Shapiro et al. (1997) and linked to the migration of the hypocenters over time, allows us to associate the swarms' temporal duration with the rocks' permeability characteristics. Swarms characterized by long durations (years) and low diffusivity values (10^{-3}-10^{-2} m^2/sec) are associated with low permeability fault systems. On the contrary, shorter durations (days) and high diffusivity values (0.5-1 m^2/sec or greater) indicate the presence of highly permeable systems in which seismicity is induced by the rise of fluids at high pressures (Amezawa et al., 2021). We focus on the clustered seismicity in the central-southern Apennines, which extends from the south of L'Aquila to Benevento, to analyze the spatio-temporal characteristics of the swarms and the relationship between their temporal duration and diffusivity.

Compared to the rest of the chain, this sector is characterized by (1) low seismicity rates, which do not allow us to follow the evolution of seismicity and the mechanisms underlying it, and (2) a high seismic risk, as demonstrated by the strongest and most destructive sequences recorded within the historical catalogs which magnitude M ~ 7.

We analyzed the seismicity reported in the catalog of absolute locations CLASS (Latorre et al., 2022), which describes Italian seismic activity over the past 37 years (1981-2018). Additionally, we augmented the catalog within a 7-year time window (2012-2018) using a template matching technique (Vuan et al., 2018). This choice was made based on the optimal distribution and operation of the seismic network. The initial catalog is improved, lowering the completeness magnitude by more than one degree (+ 20,000 events with -1.5<M<5.0). This approach allowed the analysis and comparison of clustered seismicity in two catalogs with different time extensions and resolutions.

Clustered seismicity is defined relative to the background using a nearest-neighbor technique (Zaliapin & Ben-Zion, 2020). Due to the great spatio-temporal variability of the seismic

phenomenon, no univocal methods in the literature can establish the spatial dimension and duration of the single cluster. The low seismicity rates of this area require a very detailed analysis on a small space-time scale and different methodological approaches. For the spatial definition, we used the Kernel Density calculation to determine an event's density probability in each radius. The time duration is defined using the approach described by Roland et al. 2009 based on the evaluation of the percentage of seismicity rate.

We identified 53 polyphasic seismic clusters in the complete catalog (37-year time window), and 30 in the improved catalog (7-year time window). The clusters were subsequently divided into swarms and sequences. The diffusivity was calculated for each cluster using the Shapiro et al. (1997) relationship.

Most of the seismicity is expressed as swarm-type and characterized by high diffusivity values (≥ 1m^2/sec) with short temporal durations (days-months). This result confirms that the clustered seismicity is linked to highly permeable fault zones and the natural injection of fluids under pressure. The swarms present in this sector of the Apennine chain can, therefore, be linked to the deep migration of CO2-rich fluids (Chiodini et al., 2004), which exploit pre-existing fault zones as a preferential path.

References

Amezawa Y., Taeta T., Kosuga M. (2021) Migration difusivity as a controlling factor in the duration of earthquake swarms;https://doi.org/10.1186/s40623-021-01480-7

Chiodini, G., C. Cardellini, A. Amato, E. Boschi, S. Caliro, F. Frondini, and G. Ventura (2004). Carbon dioxide Earth degassing and seismogenesis in central and southern Italy, Geophys. Res. Lett., 31, L07615. doi: 10.1029/2004GL019480

Latorre D., Di Stefano R., Castello B., Michele M., Chiaraluce L. (2022) Catalogo delle Localizzazioni ASSolute (CLASS): locations (Version 1). Istituto Nazionale di Geofisica e Vulcanologia (INGV). https://doi.org/10.13127/class.1.0

Roland E., Mc Guire J.J. (2009) Earthquake swarms on transform faults https://doi.org/10.1111/j.1365-246X.2009.04214.x

Shapiro A.S., Huenges E., Borm G. (1997) Estimating the crust permeability from fluid-injection-induced seismic emission at the KTB site https://doi.org/10.1111/j.1365-246X.1997.tb01215.x

Vuan A., Sugan M., Amati G., Kato A. (2018). Improving the Detection of Low-Magnitude Seismicity Preceding the Mw 6.3 L'Aquila Earthquake: Development of a Scalable Code Based on the Cross Correlation of Template Earthquakes.doi:10.1785/0120170106

Zaliapin, I., & Ben-Zion, Y. (2020). Earthquake declustering using the nearest-neighbor approach in space- time-magnitude domain. Journal of Geophysical Research: Solid Earth, 125, e2018JB017120. https://doi.org/ 10.1029/2018JB017120

Author: gemmacipressi@gmail.com

HOW ELASTIC IS ELASTIC DEFORMATION (IN GREENLAND)?

A. Consorzi, D. Melini, G. Spada

Glacial Isostatic Adjustment (GIA) is the time-dependent response of the Earth to spatio-temporal variations of surface loads. Since the seminal work of Wu and Peltier (1982), the GIA community has customarily adopted rheological models including a fluid core, a viscoelastic mantle and an elastic lithosphere. As a matter of fact, the focus of GIA modelling has always been the mantle viscoelastic rheology, that is the main driver of the deformation on the millennial timescale. This is motivated by the large size of the Late-Pleistocene ice sheets, which induce deformations that are mainly sensitive to the Earth's bulk properties. Presently, the highest rates of GIA deformation are measured in locations like Greenland, North America and Antarctica (Kremeer et al. 2018, Khan et al. 2016), where glaciers or ice sheets are still present. These ice masses are experiencing, in addition to the regular cycle of seasonal accumulation and ablation, a net loss caused by climate change (Osatoka et al. 2022). For this reason, GNSS stations located in the proximity of these glaciers are sensitive not only to the GIA-induced displacement but also to the elastic response of the lithosphere. Relatively small ice loads are expected to drive deformations that sense the fine structure of the Earth's outermost layers.

Even though it is undeniable that the lithosphere presents an elastic behaviour with respect to the underlying mantle, it is also true that *elasticity* is an ideal concept. In fact, rheology is a matter of time scales and, if we focus on those of GIA, the assumption of a purely elastic lithosphere is certainly unquestionable. Nevertheless, since we now dispose of high-quality geodetic records through the GNET (Bevis et al. 2009), it should be possible to identify lags between the load time evolution and the surface response. This becomes even more important when we perform local studies: especially nearby glaciers, the contribution of local processes such as underground water drainage, porosity or permafrost variations become more important and contribute to the inelasticity of the first lithospheric layers (Durkin et al. 2019, Mordret et al. 2016). Few other works in the literature have investigated this problem concerning possible phase lag due to periodic loading (Tang et al. 2020, Liu et al. 2017). Notably, Bevis et al. (2012) show a very good correlation between the global periodic loading (air mass + ice mass) and the global displacement, but it cannot be excluded that a more local-scale study might instead show delays in the Earth's response, especially in areas in which the lithosphere is weaker.

In this work we will compare the response to sinusoidal forcings of several Earth models with different lithospheric parameters, varying the thickness, rigidity, rheology and load size. We

will also consider two parallel families of models, one with a Maxwell mantle, and a second one with an Andrade (1910) mantle. Our goal is showing the role of every parameter in the determination of the response function or, in other words, the displacement. In particular, we will try to establish which combination of forcing period and load extent leads to the largest phase lag between the load history and the consequent response. As a preliminary experiment we performed a series of tests using the Earth Model from Barletta (2006). This model presents a thin elastic lithosphere of *18.5 km* and *5* viscoelastic layers of different viscosities (see Tab. 1). Firstly, with the ALMA code (Melini et al. 2022), we analysed the complex Love Numbers *h* and *l* associated with this model. Particularly, we were interested in the phase lag, namely

$$tan(\phi) = -Im[L_n(\omega)]/Re[L_n(\omega)] .$$

This quantity is of great interest since, through the relation $\Delta t = arcsin(Q^{-1})/\omega$, where Q is the quality factor and ω the tidal angular frequency (Tobie et al. 2019) , it allows us to evaluate the time delay between the load signal and the Earth's response. Results are shown in Fig. 1, where the plots display a quite complicated behaviour: the vertical Love number *h* presents, up to degree *n = 100*, a double-peak behaviour, while for higher degrees one peak only is observed. However, it is apparent that the more substantial phase lags occur for periods within 10^0 *kyr* < *T* < 10^2 *kyr*. By looking at the horizontal Love Number instead, we can clearly distinguish that, especially for degrees n > 10 and for shorter periods ($\sim 10^{-1}$ kyr), large phase lags are still visible.

Next, using the Taboo code (Spada et al. 2004) we computed the response of the model to a single disc load of semi amplitude α *= 1.5*° with a sinusoidal time history in which the ice height fluctuated between a maximum value of *10 m* and a minimum of *0 m*. We tested the sensibility of this model to different forcing periods, and we pushed our analysis up to the harmonic degree *128*. As we can see from Fig. 2, the findings of our previous analysis are confirmed: for periods of the order of 10^0 *kyr* the time lag between the load and the surface response is clearly visible, while for shorter forcing periods only horizontal displacements seem to preserve a distinguishable time lag.

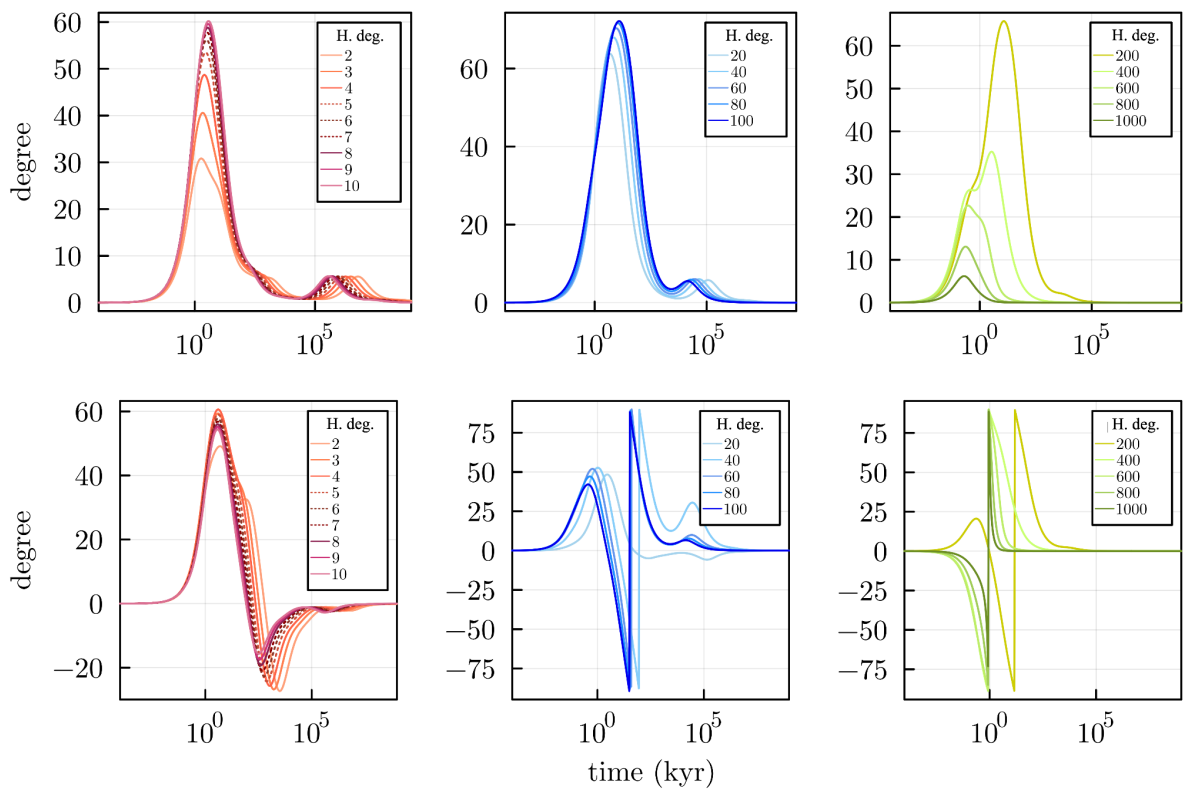

Fig. 1: Phase lag of Love numbers *h* (first row) and *l* (second row) for different harmonic degrees.

Depth (km)	Density (kg/m^3)	Rigidity (10^{10} Pa)	Viscosity (Pa · s)
6371	2650.0	2.97	$1.00 \cdot 10^{35}$
6352.5	2750.0	5.58	$2.15 \cdot 10^{19}$
6341.0	2900.0	6.81	$5.00 \cdot 10^{21}$
6331	3439.0	7.27	$4.64 \cdot 10^{20}$
5951	3882.3	10.9	$4.64 \cdot 10^{20}$
5701	4890.6	22.1	$1.00 \cdot 10^{21}$
3480	10932.0	0.00	0.00

Tab. 1: Earth model from Barletta 2006.

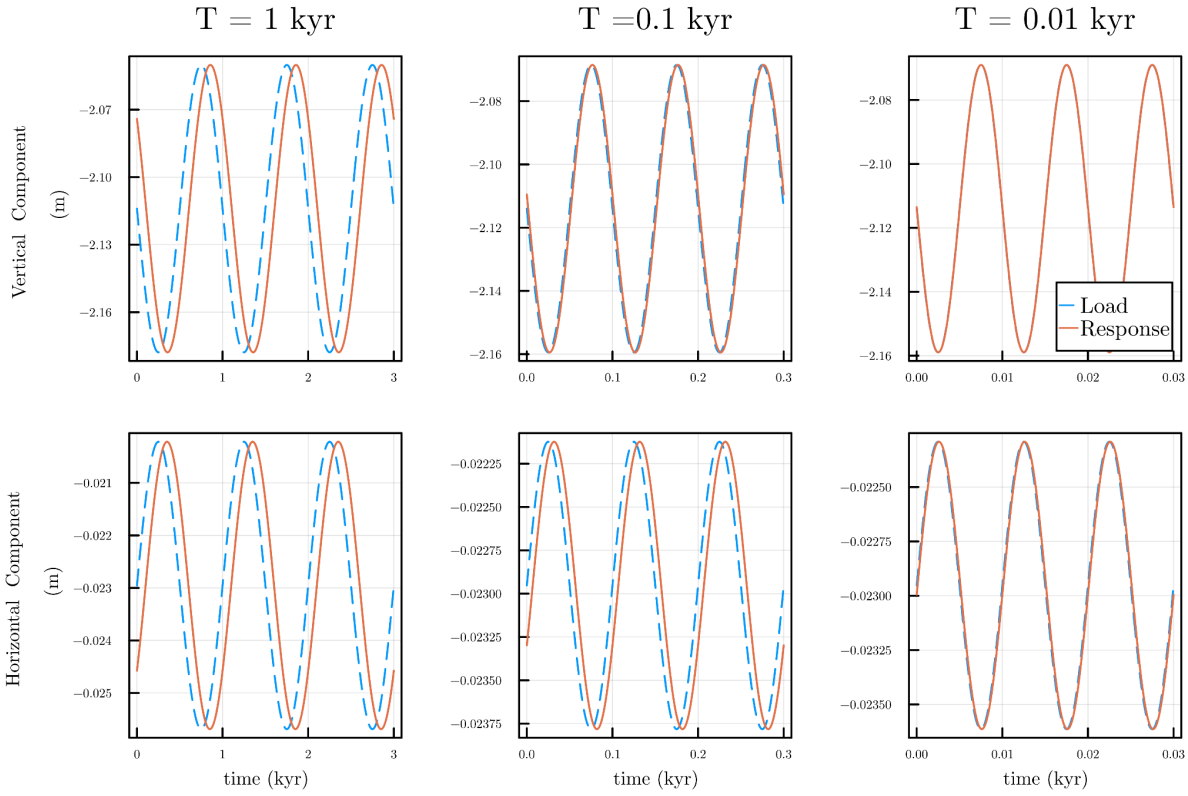

Fig. 2: Vertical (first row) and horizontal (second row) component of the displacement produced by a sinusoidal time history. The input load has been rescaled and inverted to ease the comparison between the two signals.

REFERENCES

Andrade, E. N. D. C. (1910). On the viscous flow in metals, and allied phenomena.

Proceedings of the Royal Society of London. Series A, Containing Papers of a Mathematical and Physical Character, 84(567):1–12.

Barletta, V. R., Ferrari, C., Diolaiuti, G., Carnielli, T., Sabadini, R., and Smiraglia, C. (2006). Glacier shrinkage and modeled uplift of the Alps. *Geophysical research letters*, *33*(14).

Bevis, M. G., Kendrick, E. C., Brown, A. K., Khan, S. A., Knudsen, P., Madsen, F., ...and Willis, M. J. (2009). Greenland GPS Network: Crustal oscillations and seasonal ice mass fluctuations. In *AGU Fall Meeting Abstracts* (Vol. 2009, pp. G43B-0728).

Bevis, M., Wahr, J., Khan, S. A., Madsen, F. B., Brown, A., Willis, M., ... and Francis, O. (2012). Bedrock displacements in Greenland manifest ice mass variations, climate cycles and climate change. *Proceedings of the National Academy of Sciences*, *109*(30), 11944-11948.

Durkin, W., Kachuck, S., and Pritchard, M. (2019). The importance of the inelastic and elastic structures of the crust in constraining glacial density, mass change, and isostatic adjustment from geodetic observations in Southeast Alaska. *Journal of Geophysical Research: Solid Earth, 124*, 1106–1119. https://doi.org/10.1029/2018JB016399

Khan, S. A., Sasgen, I., Bevis, M., van Dam, T., Bamber, J. L., Wahr, J., … and Munneke, P. K. (2016). Geodetic measurements reveal similarities between post–Last Glacial Maximum and present-day mass loss from the Greenland ice sheet. *Science advances*, *2*(9), e1600931.

Kreemer, C., Hammond, W. C., Blewitt, G. (2018). A robust estimation of the 3-D intraplate deformation of the North American plate from GPS. *Journal of Geophysical Research: Solid Earth*, 123, 4388–4412. https://doi.org/10.1029/2017JB015257

Liu, L., Khan, S. A., van Dam, T., Ma, J. H. Y., and Bevis, M. (2017). Annual variations in GPS-measured vertical displacements near Upernavik Isstrøm (Greenland) and contributions from surface mass loading. *Journal of Geophysical Research: Solid Earth*, *122*(1), 677-691.

Melini, D., Saliby, C., and Spada, G. (2022). On computing viscoelastic Love numbers for general planetary models: the ALMA3 code. *Geophysical Journal International,* 231(3), 1502-1517.

Mordret, A., Mikesell, T. D., Harig, C., Lipovsky, B. P., and Prieto, G. A. (2016). Monitoring southwest Greenland's ice sheet melt with ambient seismic noise. *Science advances*, *2*(5), e1501538.

Otosaka, I. N., Shepherd, A., Ivins, E. R., Schlegel, N. J., Amory, C., van den Broeke, M., ... and Wouters, B. (2022). Mass balance of the Greenland and Antarctic ice sheets from 1992 to 2020. *Earth System Science Data Discussions*, *2022*, 1-33.

Tang, H., Dong, J., Zhang, L., and Sun, W. (2020). Deformation of a spherical, viscoelastic, and incompressible Earth for a point load with periodic time change. *Geophysical Journal International*, *222*(3), 1909-1922.

Tobie, G., Grasset, O., Dumoulin, C., and Mocquet, A. (2019). Tidal response of rocky and ice-rich exoplanets. *Astronomy & Astrophysics*, 630, A70.

Spada, G., Antonioli, A., Boschi, L., Boschi, L., Brandi, V., Cianetti, S., … and Stocchi, P. (2004). Modeling Earth's post-glacial rebound.

Wu, P., Peltier, W. R. (1982). Viscous gravitational relaxation. *Geophysical Journal International*, *70*(2), 435-485.

Investigating the Tonga-Kermadec subduction zone from the study of the preparation phase of the June 15 2019 M7.2 Kermadec Islands (New Zealand) earthquake and the January 15 2022 Hunga Tonga-Hunga Ha'apai eruption

Serena D'Arcangelo, Mauro Regi, Angelo De Santis, Loredana Perrone, Gianfranco Cianchini, Maurizio Soldani, Alessandro Piscini, Cristiano Fidani, Dario Sabbagh, Stefania Lepidi, Domenico Di Mauro

The Tonga-Kermadec zone is one of the most active areas for the subduction continuous processes characterizing the area. In the recent few years, it was affected by two important geophysical events: first a strong earthquake of M7.2 on June 15 2019 with the epicentre in Kermadec Islands (New Zealand) and then an exceptional eruption of Hunga Tonga-Hunga Ha'apai volcano on January 15 2022. In order to better understand the geodynamics on the subduction area, we conducted a multi-parametric and multi-layer study on the phenomena occurred before both events basing on the lithosphere-atmosphere-ionosphere coupling (LAIC) models. We started with a seismic analysis of the earthquake sequence previous the June 15 2019 mainshock and of those anticipated the unique eruption, focusing on the circular area major affected to the preparation phase, i.e., the one defined by the Dobrovolsky strain radius. After that, we focused our attention on the atmospheric parameters generally influenced by seismic and volcanic events (skin temperature, outgoing longwave radiation, aerosol optical depth, and so on) applying the CAPRI algorithm to the ECMWF datasets to detect anomalies in their values. At the end, using the satellite data we studied the magnetic field and electron burst precipitations, looking for precursors of both events considered. All these observations together with their similarities and differences provide a better insight of the complex tectonic context. In conclusion, we reported evidence of the thermodynamic interaction between a stiff lithosphere and a more malleable asthenosphere inside the Kermadec-Tonga region. The presence of two distinct types of coupling among the geolayers was also proposed to explain the observed results.

SAR-TOOL: A new open-source software for the analysis of geospatial data in volcano-tectonic fields

S. D'Amico[1,3], F. Guglielmino[2]

[1] *Istituto Nazionale di Geofisica e Vulcanologia, Sezione Roma2, Rome, Italy*

[2] *Istituto Nazionale di Geofisica e Vulcanologia, Sezione di Catania - Osservatorio Etneo, Catania, Italy*

[3] *Department of Biological, Geological and Environmental Sciences, University of Catania, Catania, Italy*

Abstract

Since the last decade of the twentieth century, technological advancements and the availability of open-source satellite data have significantly increased geospatial analyses. Several software programs have been developed to process satellite INSAR data, including SNAP by ESA (European Space Agency), GAMMA (Wegmüller U. & Werner C.L., 1997), Sarscape, ROI_PAC/ISCE by NASA. In parallel, various algorithms have been proposed to compare, validate and integrate the satellite data with ground-based geodetic data. In particular, the SISTEM algorithm proposed by (Guglielmino et al., 2011) and based on elasticity theory, simultaneously integrates GNSS and INSAR data to provide 3D displacements maps of the study area. In order to (a) simplify the SISTEM pre-process work, (b) quickly analyse the outputs and (c) enhance the usability and ongoing development of SISTEM, we have developed SAR-TOOL, an open-source software in the Python language. Furthermore, we have developed an intuitive and lightweight GUI (Graphical User Interface), optimised to automatically adapt to different screen resolutions, ensuring an optimal user experience on any desktop, with ease of use designed especially for those without knowledge of computer programming. The GUI is structured with various frames to facilitate different operations on geospatial data, making the user interface organised and easy to navigate (Fig. 1).

From the SAR-TOOL GUI is possible:

- Visualise and convert the user's raster/vector data into various geospatial formats;
- Easily project data into various geographical reference systems;
- Crop and change the resolution of raster data;
- Homogenise input data through the development of a data intersection algorithm, which can then be supplied to the SISTEM algorithm;
- Generate synthetic data (DEM, synthetic Mogi source model (Mogi K., 1958) and synthetic GPS points) to associate with the modelled surface, in order to study the effects of inflation/deflation cycles as the parameters and position of the spherical source change (Fig. 2);

- Use the SISTEM algorithm effectively and interactively to obtain three-dimensional ground deformation maps, using one or more datasets of interferometric data as input.

SAR-TOOL utilises the open-source GDAL (Geospatial Data Abstraction Library) for the analysis of raster and vector data.

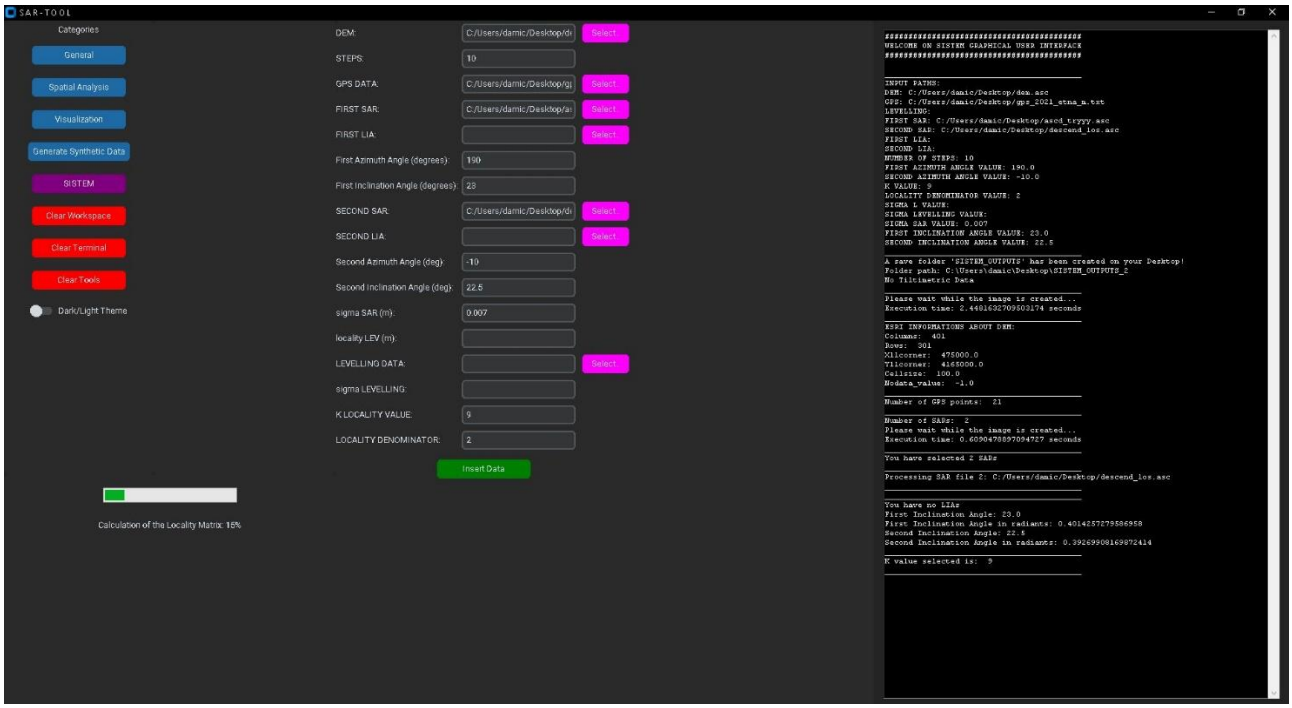

Fig. 1 - Main working screen of the open-source SAR-TOOL software. In particular, the figure shows a work session related to the interactive selection and addition of input data required by the SISTEM algorithm, featuring a terminal on the right showing both the parameters entered and those calculated by the algorithm.

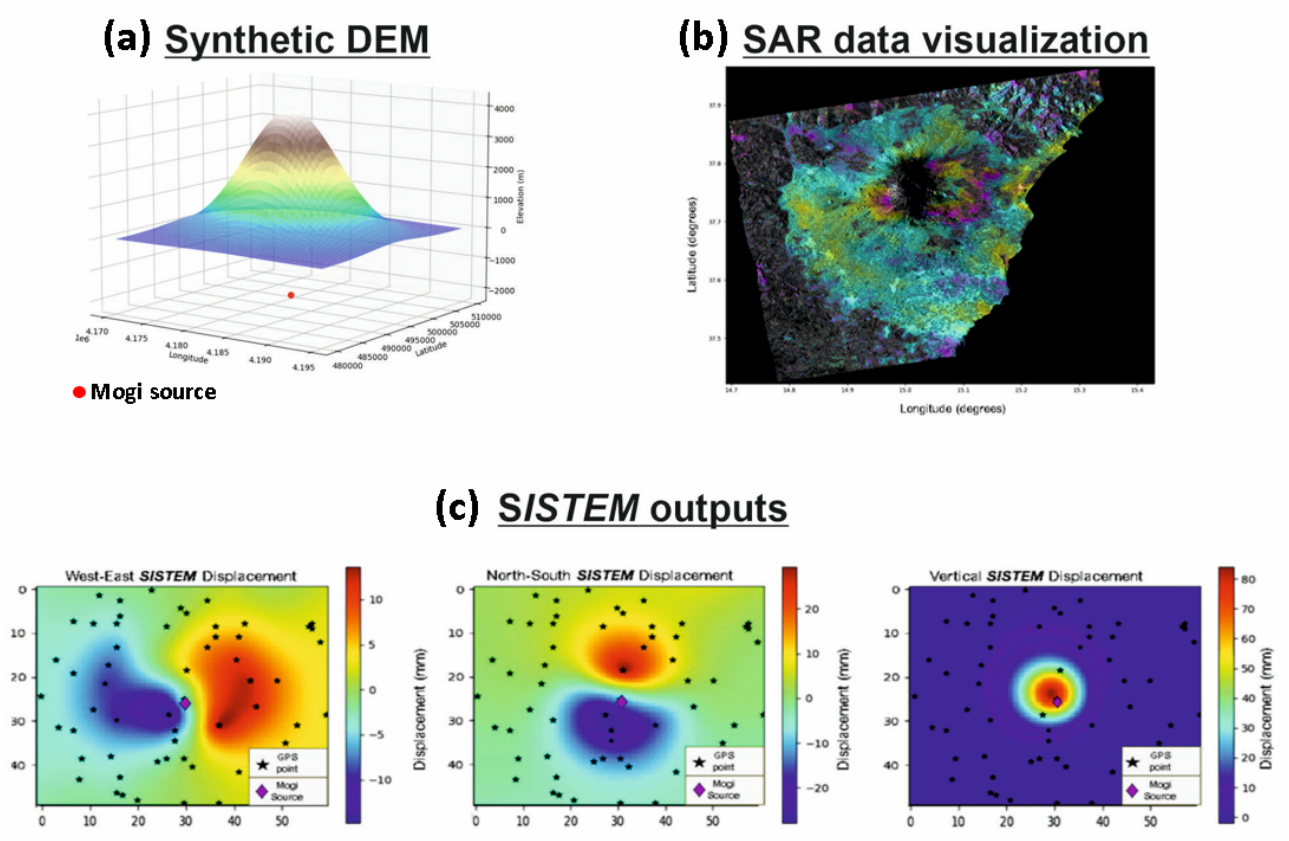

Fig. 2 - Examples of products obtained through SAR-TOOL. (a) Modelling of a synthetic DEM and a spherical Mogi source located at a depth of 2000 metres above sea level; (b) Visualisation of a phase interferogram relative to a ground deformation period at Etna volcano (Italy); (c) Output of the displacements generated by a spherical Mogi source and calculated by the SISTEM algorithm through interaction with 60 synthetic GPS points arranged in a random geometry within the grid.

References

Guglielmino F., Nunnari G., Puglisi G., Spata A.; 2011: Simultaneous and Integrated Strain Tensor Estimation from geodetic and satellite deformation Measurements (SISTEM) to obtain three-dimensional displacement maps. IEEE Trans. Geosci. Remote Sens. vol., 49, pp. 1815-1826.

Mogi K.; 1958: Relations between the eruptions of various volcanoes and the deformations of the ground surfaces around them. Bulletin of the Earthquake Research Institute, pp. 99-134.

Wegmüller U., Werner C.L.; 1997: GAMMA SAR processor and interferometry software. Proceedings 3rd ERS Scientific Symposium, Florence, Italy.

Corresponding author: salvatore.damico2@ingv.it

On constraining 3D mantle flow patterns in subduction, mid-ocean-ridge, and plume environments with teleseismic body wave data

M. Faccenda1 , B. P. VanderBeek1

[1] *Dipartimento di Geoscienze, Università di Padova, Padova, Italy*

Conventional seismic tomography studies consider the Earth's interior as mechanically isotropic, despite seismic anisotropy being widely observed. This current standard approach to seismic imaging is likely to lead to significant artefacts in tomographic images with first-order effects on interpretations and hinders the quantitative integration of seismology with geodynamic flow models. In this contribution we use geodynamic and seismological modeling to predict the elastic properties and synthetic teleseismic P- and S-wave travel-time datasets for three different tectonic settings: a plume rising in an intraplate setting, a divergent margin, and a subduction zone (Figs. 1, 2). Subsequently, we perform seismic anisotropy tomography testing a recently developed methodology that allows for the inversion of an arbitrarily oriented weakly anisotropic hexagonally symmetric medium using multiple body-wave datasets. The tomography experiments indicate that anisotropic inversions of separate and joint P- and S-wave travel-times are capable of recovering the first order isotropic velocity anomalies and anisotropic patterns. In particular, joint P- and S-wave anisotropic inversions show that by leveraging both phases it is possible to greatly mitigate issues related to imperfect data coverage common in seismology and reduce parameter trade-offs. In contrast, by neglecting seismic anisotropy, isotropic tomographic models provide no information on the mantle fabrics and in all cases are contaminated by strong velocity artifacts. In the inversions the magnitude of anisotropy (as well as that of seismic anomalies) is always underestimated owing to regularization procedures and smearing effects. It follows that the true seismic anisotropy of mantle rocks is likely higher than estimated from anisotropic tomographies, and more consistent with predictions from laboratory and numerical micro-mechanical experiments. Altogether, these results suggest that anisotropic body-wave tomography could provide unprecedented information about the Earth's deep geological structure, and that the latter could be better recovered by complementing teleseismic body-wave travel-times with other geophysical datasets (Faccenda and VanderBeek, 2023).

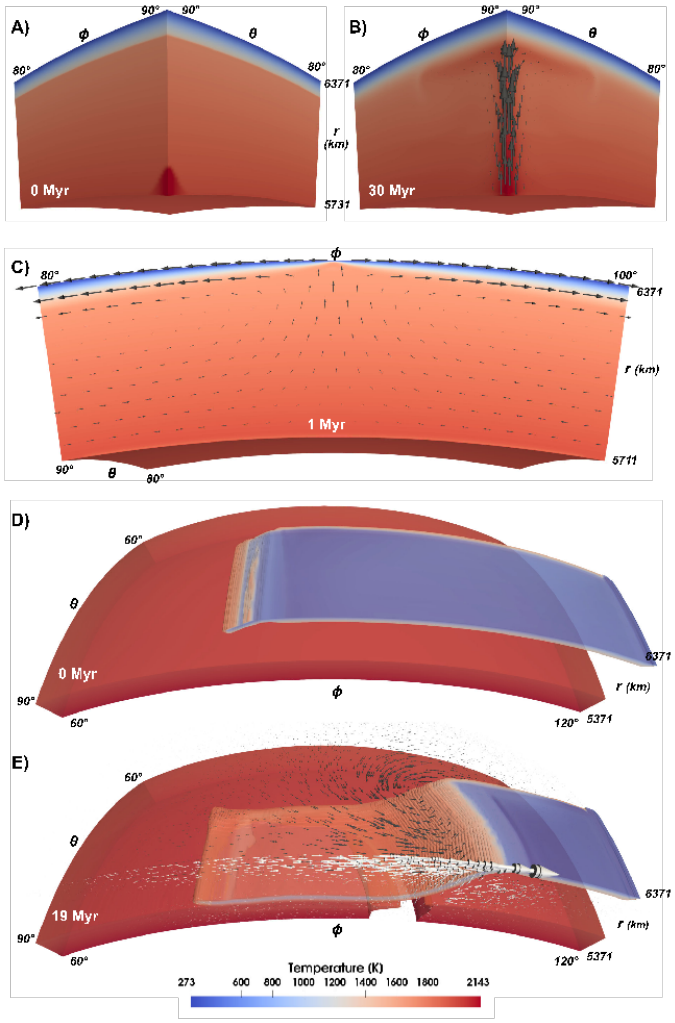

Fig. 1 – Temperature and velocity (arrows) fields for the three modeled tectonic settings as predicted by macro-scale geodynamic modeling. (A, B) Rising plume model initial setup and after 30 Myr. Only half of the computational domain (ϕ = 80° - 90°) is shown. The thermal anomaly is delimited by a 2D gaussian surface containing material at 2143 K, resulting in a 200-250 K temperature anomaly over the mantle transition zone. The 2D gaussian surface is centered at (ϕ, θ) = (90°, 90°), and has a radial extent of 1°, a horizontal standard deviation of 0.4° and a maximum amplitude of 100 km. (C) Oceanic spreading ridge model after 1 Myr. The arrows length at the surface is proportional to the imposed 2 cm/yr divergence rate. (D, E) Oceanic plate subduction model initial setup and after 19 Myr. The opaque surfaces enclose material with viscosity ≥ 10^{21} Pa s and are colored according to temperature. In (E) the white (dark grey) arrows indicate the poloidal (toroidal) component of the velocity field. The arrows length in (B) and (E) is downscaled by 10 and 4 times with respect to that in (C).

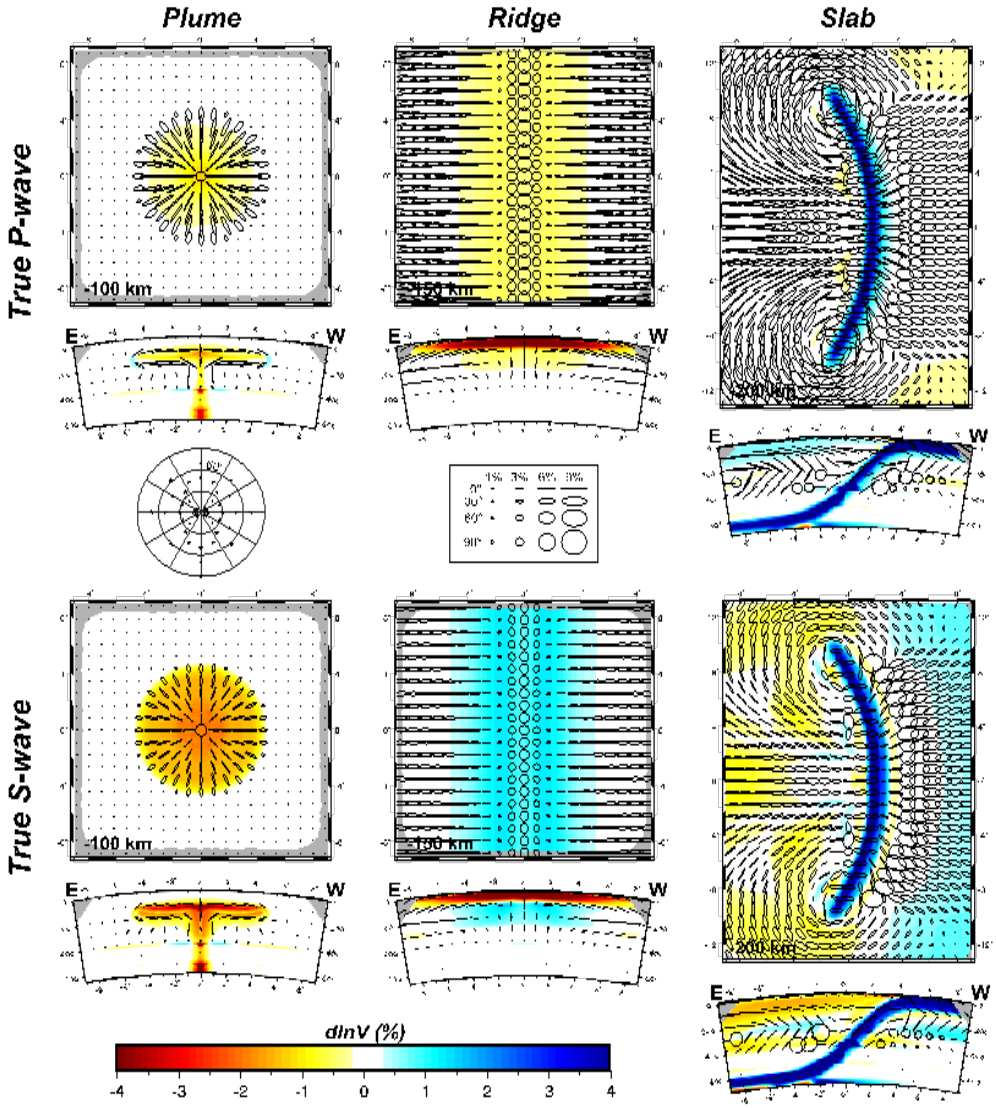

Fig. 2 - True P-wave (top two panels) and S-wave isotropic anomalies and fast symmetry axis orientations for the three modeled tectonic settings as predicted by micro-scale geodynamics modeling. Horizontal and E-W vertical cross sections (along the equatorial plane of the geodynamic model spherical domain) are shown. Velocity anomalies $\Delta\, lnV_{P,S}$ are computed (i) using the average of the three principal velocities, that for an hexagonally symmetric medium with a fast symmetry axis are V_{fast}, V_{slow}, V_{slow}, and (ii) with respect to reference radial velocity profiles taken at the corner of the computational domain with minimum the X-Z axes coordinates, which is representative of the far-field, unperturbed mantle. The P-wave low velocity and S-wave high velocity anomalies at 150 km in the ridge model, and the P-wave high velocity and S-wave low velocity anomalies in the subduction model mantle wedge, are caused by deviations from the hexagonally symmetry model. The length of the ellipses major axis is proportional to: $2f(\%) = \dfrac{\left(V_{fast} - V_{slow}\right)}{\left(V_{fast} + V_{slow}\right)} * 200\%$. The orientation of the fast symmetry axis is parallel to the major axis of the ellipses, while the length of minor axis is proportional to the dip relative to the cross section.

References

Faccenda, M., VanDerBeek, B.P., On constraining 3D seismic anisotropy in subduction, mid-ocean-ridge, and plume environments with teleseismic body wave data. J. Geodyn., 158, https://doi.org/10.1016/j.jog.2023.102003 (2023).

Corresponding author: manuele.faccenda@unipd.it

A dynamic identification of *continuous discontinuities* in geodynamic numerical models

V. Fedeli[1], A.M. Marotta[1]

[1] Dipartimento di Scienze della Terra "Ardito Desio" (Università degli Studi di Milano, Italy)

Discontinuities affect the Earth's dynamics, yet the Earth is often represented in geodynamical models as a continuous material. The challenge of representing discontinuities in numerical models has been addressed in several ways in literature. The split node method, originally introduced by Jungels (1973) and Jungels and Frazier (1973) for elastic rheology and then modified by Melosh and Raefsky (1981) to simplify its implementation, allows the introduction of discontinuity into a finite element model by imposing an a-priori slip at a designated node, where the displacement depends on the element which the node is referred to. Originally, this method requires that the discontinuity's geometry and slip are pre-established.

More recently, Marotta et al. (2020) modify this approach by introducing a coupling factor that indicates the percentage difference between the velocities of the element to which the slip node belongs, while the velocity consistently derives from the dynamic evolution of the system. However, this method still requires the pre-establishment of the discontinuity's geometry.

We here present a new technique that enables the dynamic identification of the discontinuity's during the thermomechanical evolution of the system, based on physical parameters and without predefining the slip or the geometry.

We have implemented a new algorithm that identifies one or more discontinuities in a finite-element scheme operating through two phases: nucleation and propagation. Nucleation involves selecting a yield physical property and identifying the potential slip nodes, i.e., nodes on which the chosen physical property exceeds a yield value. The nucleus is then identified as the potential slip node where the chosen property most exceeds the yield. Propagation can be performed by choosing between three approaches of propagation: single simple fault, multiple simple fault and single double fault; and three schemes for the identification of neighboring nodes: grid-bounded, pseudo-free and free. The resulting discontinuity is the line connecting the nucleus and the propagation nodes. Once the discontinuity has been identified, a coupling factor is introduced and the algorithm continues to operate following the Marotta et al., (2020)'s scheme.

The results of several benchmark tests, performed through both simple and complex finite-elements models, confirm the success of the algorithm in recognizing yield conditions and introducing a discontinuity into a finite-element model and demonstrate the correctness of the propagation's geometry.

References

Jungels P.H.; 1973: Models of tectonic processes associated with earthquakes. PhD thesis.

Jungels P.H., Frazier G.A. Frazier; 1973: Finite element analysis of the residual displacements for an earthquake rupture: source parameters for the San Fernando earthquake. Journal of Geophysical Research.

Marotta A.M., Restelli F., Bollino A., Regorda A., Sabadini R.; 2020: The static and time-dependent signature of ocean-continent and ocean-ocean subduction: The case studies of Sumatra and Mariana complexes. Geophysical Journal International.

Melosh H.J., Raefsky A.; 1981: A simple and efficient method for introducing faults into finite element computations. Bulletin of the Seismological Society of America.

Corresponding author: valeria.fedeli@unimi.it

PRIN 2020 NASA4SHA Project: A Combined Regional Velocity Field of Northern Italy

A. Galvani1, M. Albano1, C. Braitenberg2, F. Brighenti3, R. Caputo4, F. Carnemolla3, D. Cheloni1, G. De Guidi3, R. Devoti1, A. Magrin5, A. Pellegrinelli4, G. Pietrantonio1, G. Rossi5, S. Stramondo1, L. Tunini5, D. Zuliani5

[1] Istituto Nazionale di Geofisica e Vulcanologia, Rome, Italy
[2] Università degli Studi di Trieste, Trieste, Italy
[3] Università degli Studi di Catania, Catania, Italy
[4] Università degli Studi di Ferrara, Ferrara Italy
[5] Istituto Nazionale di Oceanografia e di Geofisica Sperimentale, Trieste, Italy

The activity presented in this note is part of the PRIN 2020 NASA4SHA Project (Fault segmentation and seismotectonics of active thrust systems: the Northern Apennines and Southrn Alps laboratorie for new Seismic Hazard Assessments in northern Italy). The project's objective is to define, through a multidisciplinary approach including geological, geophysical, seismological, paleoseismological, and geodetic methods at various scales (regional and local), the geometry and kinematics of the main compressive systems in the central – estern Southern Alps and Northern Apennines (Fig. 1).

Geodetic methods make it possible to reconstruct the ongoing deformation rate of the Earth's surface at regional and local scales (with high-density networks). This information, combined with the 3D model of tectonic structures present in the investigated region, can indicate areas/volumes where the tectonic activity and the deformation are either more or less intense, enabling a focus on fault zones where the stress is increasingly accumulated.

We analyzed data from continuous GNSS (Global Navigation Satellite Systems) stations covering the entire study area, belonging to the RING (Rete Integrata Nazionale GNSS) and FReDNet (Friuli Regional Deformation Network) networks, managed by INGV (Istituto Nazionale di Geofisica e Vulcanologia) and OGS (Istituto Nazionale di Oceanografia e di Geofisica Sperimentale - OGS) respectively, together with data from other permanent networks, managed by various institutions. In addition, we have resurveyed some vertices of the IGM95 geodetic network, focusing on local transects orthogonal to the main compressive structures, and we have analyzed the new discontinuous GNSS observations together with the previous ones performed in the past by IGM (Istituto Geografico Militare) on the same vertices.

Here, we present the regional velocity field (Fig. 2) of the GNSS permanent stations (discontinuous sites will be included in a second release), obtained as a result of the combination of two velocity

fields calculated by INGV and OGS, with different analysis softwares, Bernese and Gamit Globk

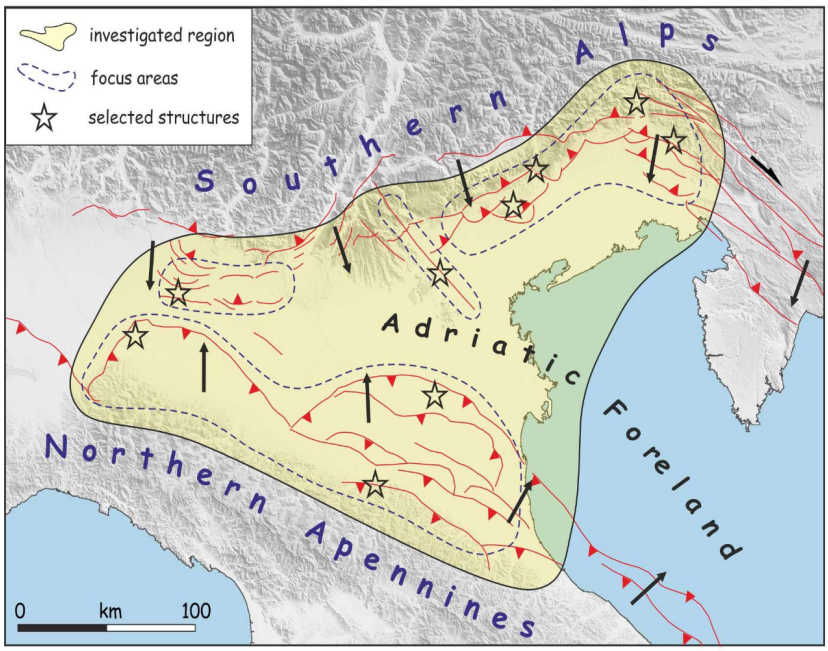

Fig. 1 – Map of the study area of the PRIN 2020 NASA4SHA Project.

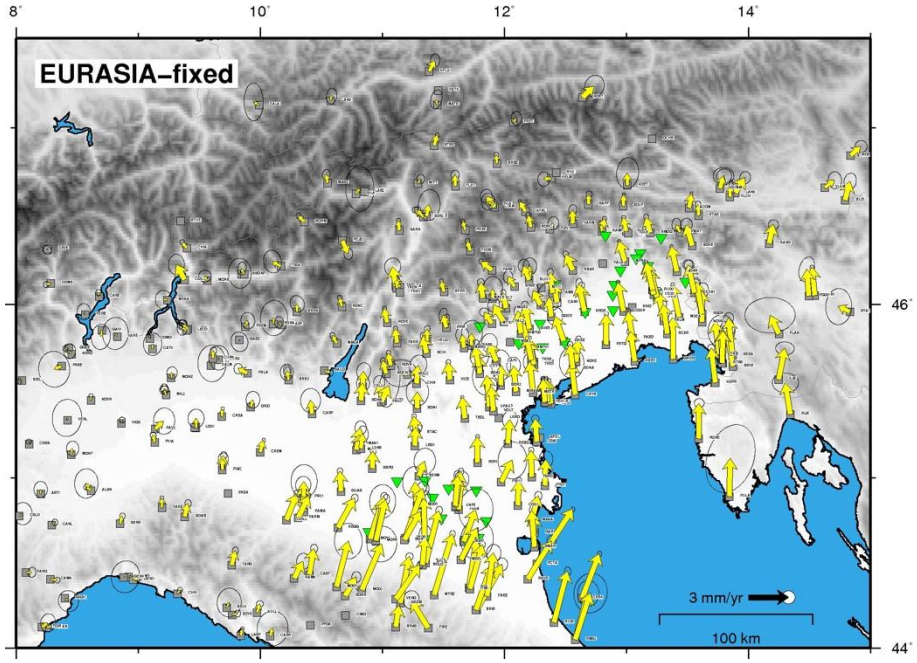

Fig. 2 – Map of the horizontal GNSS velocities in the Eurasian-fixed reference frame, from the combined solution. Error ellipses at 95%. The inverted green triangles are the locations of the resurveyed vertices of the IGM95 network.

respectively. The velocity field is expressed in the ITRF2014 reference frame, with respect to the Eurasian plate (Altamimi et al., 2017). The combination procedure described in Devoti et al., 2017, is based on a linear least-squares approach, where we consider each velocity field as a sample of the true velocity field and the combined velocity as the best estimate of the true velocity field. The combined solution allows a validation of the velocity field by assessing the velocity repeatability of velocities at the common sites and minimize the probability of including biased velocities.

The combined long-term horizontal velocity field is then used for obtaining the strain-rate field across the active deformation zones, by applying the classic approach based on GNSS velocity vectors converted in the strain-rate field (e.g., Beavan and Haines, 2001; Shen-Tu, 1998).

References

Altamimi Z., Métivier L., Rebischung P., Rouby H., Collilieux X.; 2017: ITRF2014 plate motion model, Geophys. J. Int., 209, 3, doi:10.1093/gji/ggx136.

Beavan J., Haines J.; 2001: Contemporary horizontal velocity and strain rate fields on the Pacific-Australian plate boundary zone through New Zealand. J. Geophys. Res., 106(B1), doi:10.1029/2000JB900302.

Devoti R., D'Agostino N., Serpelloni E., Pietrantonio G., Riguzzi F., Avallone A., Cavaliere A., Cheloni D., Cecere G., D'Ambrosio C., Falco L., Selvaggi G., Mètois M., Esposito A., Sepe V., Galvani A., Anzidei M.; 2017: A Combined Velocity Field of the Mediterranean Region. Annals of Geophysics, 60(2), doi:10.4401/ag-7059.

Shen-Tu B., Holt W.E., Haines J.; 1998: Contemporary kinematics of the western United States determined from earthquake moment tensors, very long baseline interferometry, and GPS observations. J. Geophys. Res., 103(B8), doi:10.1029/98JB01669.

Corresponding author: alessandro.galvani@ingv.it

Strength of the lithosphere derived by geological and geophysical data: the Graham Land (Antarctic Peninsula) case study

F. Linsalata[1], D. Melini[2], G. Spada[1]

[1] Dipartimento di Fisica e Astronomia (DIFA), Alma Mater Studiorum Università di Bologna, Italy
[2] Istituto Nazionale di Geofisica e Vulcanologia (INGV), Roma, Italy

One-dimensional lithospheric strength is usually represented by a diagram of shear-stress versus depth (Brace, 1980), known as the Brace-Goetze strength profile, or Yield Strength Envelope (YSE). The shape of this diagram, informally dubbed the 'Christmas tree', strongly depends on the composition of the constituent rocks. This constitutive property is usually extrapolated from centimeter-sized laboratory samples (e.g. Hirth and Kohlstedf, 2003; Zhang and Karato, 1995), from structural studies of naturally deformed rocks (e.g. Twiss, 1977; Tullis, 2002; Evans, 2005), or from a larger-scale perspective (e.g. Thatcher, 1983; Bird and Kong, 1994; Handy and Brun, 2004; Thatcher, 2009). However, the strength of the Earth's lithosphere has been debated since the beginning of the last century (Tesauro et al., 2009), when the concept of a strong lithosphere overlying a viscous asthenosphere was first introduced (Barrell, 1914). This concept played a major role in the development of plate tectonics (Le Pichon et al., 2013), and how the strength of the plates varies spatially and temporally is a fundamental question in geology and geodynamics (Jackson, 2002; Burov and Watts, 2006).

Yield Strength Envelopes have been calculated over the last few decades for a number of locations in Europe (e.g. Cloetingh and Burov, 1996; Cloetingh et al., 2005), America (Liu and Zoback, 1997) and Asia (Zang et al., 2007), but are not available on a regional scale for Antarctica. In this work, based on previously published data, we explore the strength of the lithosphere beneath the Graham Land region (Antarctic Peninsula, Fig. 1) using numerical modeling which simulates lithospheric deformation as a function of geological and geophysical parameters.

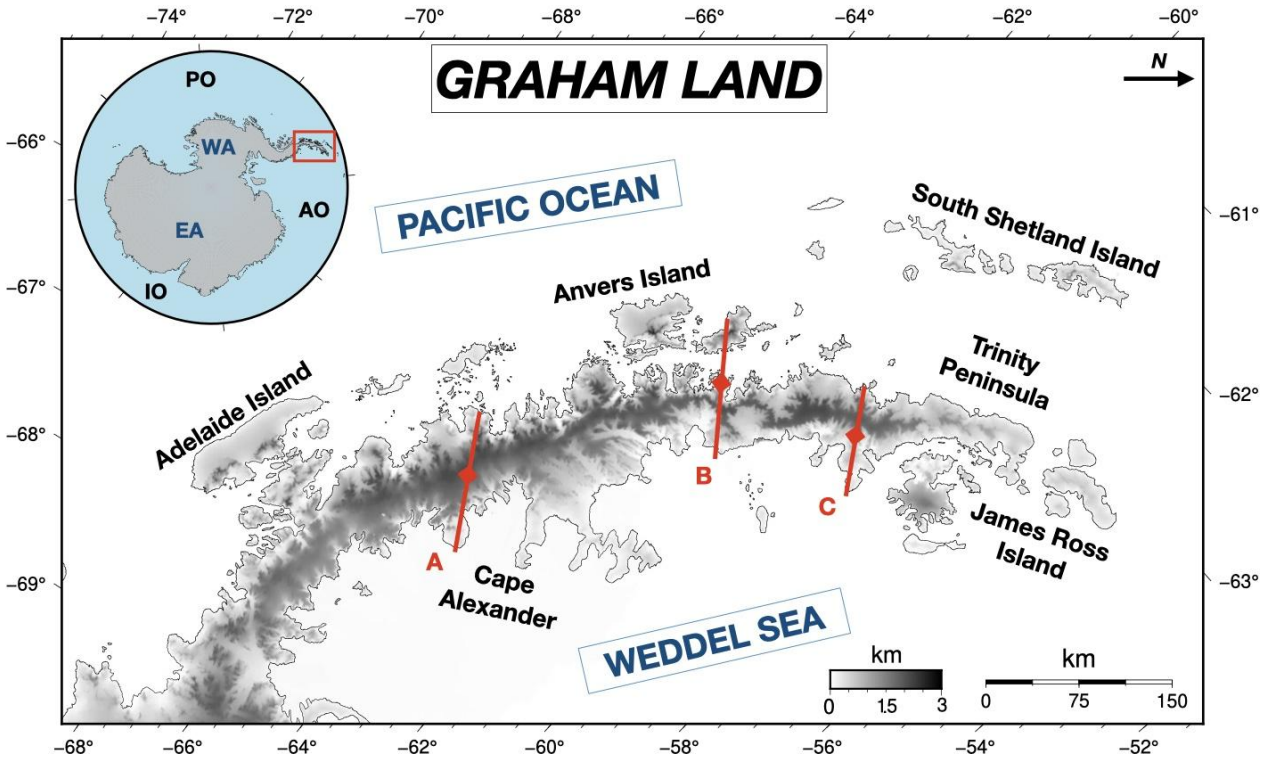

Figure 1. Detail of the study region, the Graham Land (Antarctic Peninsula) with major island. The red lines (A, B and C) indicate the location of three profiles considered in this study. The gray scale represents topography according to Global Earth Relief Grids (15 arc second). In the upper left frame, overview of the Antarctic continent with the study area highlighted by the red box. WE: West Antarctica, EA: East Antarctica, PO: Pacific Ocean, AO: Atlantic Ocean and IO: Indian Ocean.

First, we use the MIDAS algorithm (Blewitt, 2016) to process 21 GNSS time series spanning 1997–2022, provided by the Nevada Geodetic Laboratory, and we produce a robust tectonic velocity solution. Then, we calculate a new geodetic strain rate model using the VISR code (Shen et al., 1996; Shen et al., 2015), with an optimal mesh grid definition of 0.5x0.5 degrees, that best fits our study area. Second, we combine our new geodetic strain rate model with the Moho depth and rheological parameters (Tab. 1), such as Geothermal Heat Flow (GHF), heat production and thermal conductivity previously published in the literature to determine the YSE beneath Graham Land. We performed several numerical experiments in which the GHF and the rheological parameters were varied to compute predictions of the YSE. We explored the range of uncertainty in each parameter by a trial-and-error procedure with discrete sampling steps. Each combination of GHF and temperature coefficient for creep rheology constitutes an independent simulation. For each combination, the model predictions were computed with a MATLAB code; a flowchart illustrating our modeled workflow is shown in Fig. 2. The results of our study demonstrate that the “jelly sandwich” and the “crème brûlée” models are both valid for the Graham Land lithosphere, depending on specific thermal and rheological conditions considered.

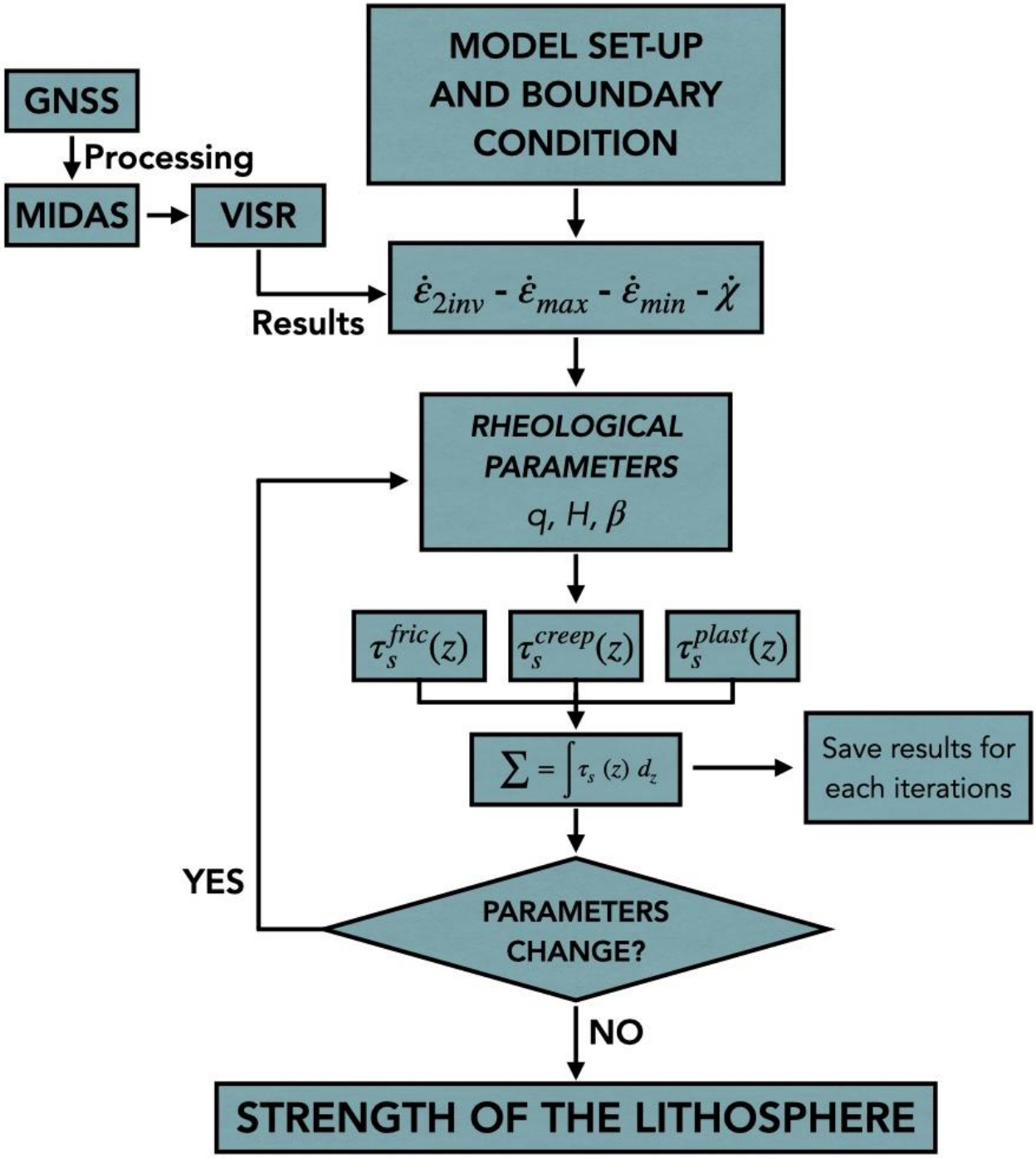

Figure 2. Modeling workflow adopted in our MATLAB Conde

Data availability statement

The MIDAS algorithm code is available from the Nevada Geodetic Laboratory (NGL) at the link http://geodesy.unr.edu/MIDAS_release/?C=M;O=A. Program to compute the strain rate is available from the Zheng-Kang Shen webpage at http://scec.ess.ucla.edu/~zshen/visr/. The numerical code implemented in MATLAB and the data underlying all figures shown in this work are available upon request from the corresponding author.

Acknowledgements

All figures have been drawn using the Generic Mapping Tools (GMT) of Wessel and Smith (1998). We acknowledge Nevada Geodetic Laboratory for making available the GPS data from the web http://geodesy.unr.edu/index.php and MIDAS software at the page http://geodesy.unr.edu/MIDAS_release/?C=M;O=A.

References

Barrell, J.; 1914. *The strength of the Earth's crust part I. Geologic tests of the limits of strength*. The Journal of Geology, 22(1), 28-48.

Bird, P., Kong, X.; 1994. *Computer simulations of California tectonics confirm very low strength of major faults*. Geological Society of America Bulletin, 106(2), 159-174.Blewitt, G., Kreemer, C., Hammond, W. C., & Gazeaux, J.; 2016. *MIDAS robust trend estimator for accurate GPS station velocities without step detection*. Journal of Geophysical Research: Solid Earth, 121(3), 2054-2068.Brace, W. F., Kohlstedt, D. L.; 1980. *Limits on lithospheric stress imposed by laboratory experiments*. Journal of Geophysical Research: Solid Earth, 85(B11), 6248-6252.

Burov, E. B., Watts, A. B; 2006. *The long-term strength of continental lithosphere: "jelly sandwich" or" crème brûlée"?*. Geological Society of America Today, 16(1), 4.

Cloetingh, S., Burov, E. B; 1996. *Thermomechanical structure of European continental lithosphere: constraints from rheological profiles and EET estimates*. Geophysical Journal International, 124(3), 695-723.

Cloetingh, S., Ziegler, P. A., Beekman, F., Andriessen, P. A. M., Hardebol, N., Dezes, P.; 2005. *Intraplate deformation and 3D rheological structure of the Rhine Rift System and adjacent areas of the northern Alpine foreland*. International Journal of Earth Sciences, 94, 758-778.

Evans, B.; 2005. *Creep constitutive laws for rocks with evolving structure*. Geol Soc Lond Spec Publ 245 (1): 329–346.

Handy, M. R., Brun, J. P.; 2004. *Seismicity, structure and strength of the continental lithosphere*. Earth and Planetary Science Letters, 223(3-4), 427-441.

Hirth, G., Kohlstedf, D.; 2003. *Rheology of the upper mantle and the mantle wedge: A view from the experimentalists*. Geophysical monograph-american geophysical union, 138, 83-106.

Jackson, J. A; 2002. *Strength of the continental lithosphere: time to abandon the jelly sandwich?*. Geological Society of America Today, 12, 4-10.

Le Pichon, X., Francheteau, J., Bonnin, J., X.; 2013. *Plate tectonics* (Vol. 6). Elsevier.

Liu, L., Zoback, M. D.; 1997. *Lithospheric strength and intraplate seismicity in the New Madrid seismic zone*. Tectonics, 16(4), 585-595.

Shen, Z. K., Jackson, D. D., Ge, B. X; 1996. *Crustal deformation across and beyond the Los Angeles basin from geodetic measurements*. Journal of Geophysical Research: Solid Earth, 101(B12), 27957-27980.

Shen, Z. K., Wang, M., Zeng, Y., Wang, F; 2015. *Optimal interpolation of spatially discretized geodetic data*. Bulletin of the Seismological Society of America, 105(4), 2117-2127.

Tesauro, M., Kaban, M. K., Cloetingh, S. A; 2009. *A new thermal and rheological model of the European lithosphere*. Tectonophysics, 476(3-4), 478-495.

Thatcher, W.; 1983. *Nonlinear strain buildup and the earthquake cycle on the San Andreas fault*. Journal of Geophysical Research: Solid Earth, 88(B7), 5893-5902.

Thatcher, W.; 2009. *How the continents deform: The evidence from tectonic geodesy*. Annual Review of Earth and Planetary Sciences, 37, 237-262.

Tullis, J.; 2002. *Deformation of granitic rocks: experimental studies and natural examples*. Reviews in Mineralogy and Geochemistry, 51(1), 51-95.

Twiss, R. J.; 1977. *Theory and applicability of a recrystallized grain size paleopiezometer*. Stress in the Earth, 227-244.

Wessel P., Smith W. H.; 1998: *New, improved version of Generic Mapping Tools released*, Eos, Transactions American Geophysical Union, 79(47), 579-579.

Zhang, S., Karato, S. I.; 1995. *Lattice preferred orientation of olivine in simple shear deformation and the flow geometry of the upper mantle of the Earth*. Nature, 375, 774-777.

Zang, S. X., Wei, R. Q., Ning, J. Y.; 2007. *Effect of brittle fracture on the rheological structure of the lithosphere and its application in the Ordos*. Tectonophysics, 429(3-4), 267-285.

Corresponding author: f.linsalata91@gmail.com, fernando.linsalata2@unibo.it

The coda attenuation method reveals a very high attenuating crust in the High Agri Valley (Southern Italy)

S. Lucente[a], V. Serlenga[b], S. de Lorenzo[a], E. del Pezzo[c,d], M. Filippucci[a,c], T. Ninivaggi[e], T.A. Stabile[b], A. Tallarico[a,c]

[a] *Università degli Studi di Bari Aldo Moro, Dipartimento di Scienze della Terra e Geoambientali, Bari, Italy*
[b] *CNR Institute of Methodologies for Environmental Analysis, IMAA, Tito Scalo, Italy*
[c] *Istituto Nazionale di Geofisica e Vulcanologia, Sezione di Napoli "Osservatorio Vesuviano", Napoli, Italy*
[d] *Instituto Andaluz de Geofisica, Universidad de Granada, Granada, Spain*
[e] *Istituto Nazionale di Geofisica e Vulcanologia, Sezione Irpinia, Grottaminarda, Italy*

High Agri Valley is an intermontane basin located in the axial portion of Southern Apennines, a fold and thrust chain originated starting from the late Oligocene (Patacca & Scandone, 2007). The investigated area is characterized by a very strong seismogenic potential as testified by the Mw=7.0 1857 earthquake. In the last decades, a low magnitude natural seismicity has been recorded by the stations belonging to both the trigger-mode monitoring network managed by ENI Oil Company and the Italian National Seismic Network managed by INGV. In addition to the natural seismicity, two anthropogenic seismicity clusters are documented (Stabile et al., 2014; Improta et al., 2017 among the others), located NE and SW of the artificial Pertusillo lake, respectively: a) fluid-induced microseismic swarms due to the injection, through the Costa Molina 2 well, of the wastewater produced by the exploitation of the Val d'Agri oilfield; b) protracted reservoir induced seismicity (RIS) caused by the combined effects of the water table oscillations of the Pertusillo lake, the regional tectonics and likely the poroelastic/elastic stress due to aquifers in the carbonate rocks (Picozzi et al., 2022). In order to gain insights on the attenuation properties of the crust of this region, we selected a dataset of about 1800 events acquired from 2001 to 2015 by the two above mentioned seismic networks, with local magnitude (ML) ranging from 0 to 3.3. The dataset is composed of triaxial recordings acquired by an average number of 14 stations.

We estimated the attenuation of S-coda waves Qc^{-1} from a linear regression analysis of the envelope of the amplitude decay curve (Sato, 1977). This parameter can give information about the physical state of the crust (possible presence of fluids, or thermal anomalies, or ductile rock volumes) and in tectonic context it is widely accepted that Q_c, estimated with the single scattering model at long lapse time, is representative of the intrinsic attenuation Q_i (Mayor et al. 2016). The method consists in the linear fitting of the decreasing trend on the envelopes of S coda waves in a selected time window. Moreover, we developed a method aimed at automatically finding the end-time (T_2) of the coda envelope, avoiding the manual and subjective criterion of selection of the end of coda. This method was tested on a significant sample of real data before of its application to the entire dataset. Only the components, for which the condition $T_1<T_L<T_2$ was fulfilled, were considered for the linear regression.
The Qc estimates were performed by using different time windows for the envelope fitting, starting from the time T_1 to the time T_L (the lapse time). In detail, we adopted, as T_1, 1.0*Ts, 1.5*Ts and 2.0*Ts (being Ts the S wave arrival time), and as T_L 10s, 15s, 20s, 25s and 30 s from the event origin

time. To evaluate the dependence of Q_c on frequency f, we filtered all the traces in bands centered around 1, 2, 3, 4, 5, 6, 8, 10, 12, 14 and 16 Hz of frequency (as suggested by Bianco et al., 2002, for Southern Apennines).

The obtained results show the increase of Q_c with f at all the considered T_L (Fig. 1). This dependence could be described by the general relation:

$$Q_c(f) = Q_0 f^{\alpha} \qquad (1)$$

where Q_0 is the Q_c at 1 Hz and α is the attenuation exponent. Our results show that in the High Agri Valley Q_0 ranges between 8 and 57, whereas α ranges between 0.66 and 1.14, indicating that the region is tectonically and seismically active, as found in other adjacent areas (Filippucci et al., 2021 and references therein). Compared with other tectonic regions worldwide, in the High Agri valley $Q_c(f)$ is very low at all the investigated frequencies (Fig. 2). This evidence could be interpreted as due to the fluid presence in the investigated crust, thus providing a further hint on the possible role of fluids in the seismicity of the area. A complete characterization of seismic attenuation of the studied area will require further investigations, that is the separation of scattering and intrinsic contributions in the total attenuation and a 3D imaging to highlight the possible relation between spatial attenuation anomalies and seismicity distribution in the investigated area.

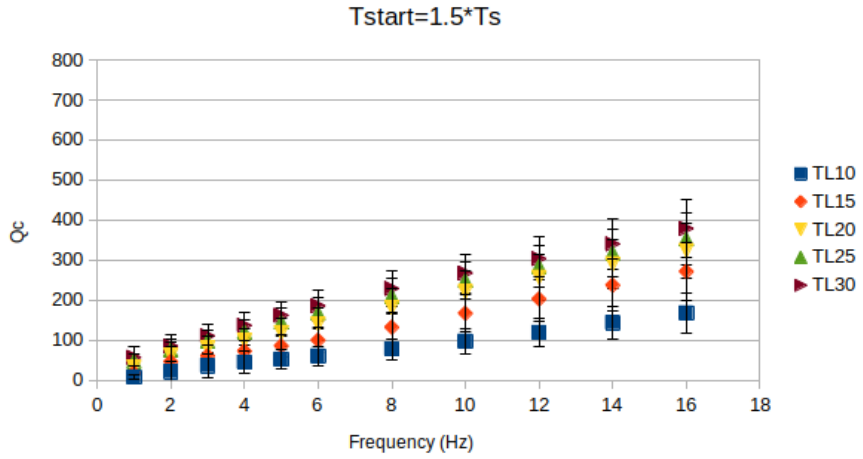

*Fig. 1 –Q_c distribution related to several time windows, starting from 1.5*Ts and ending at 10, 15, 20, 25 and 30 s.*

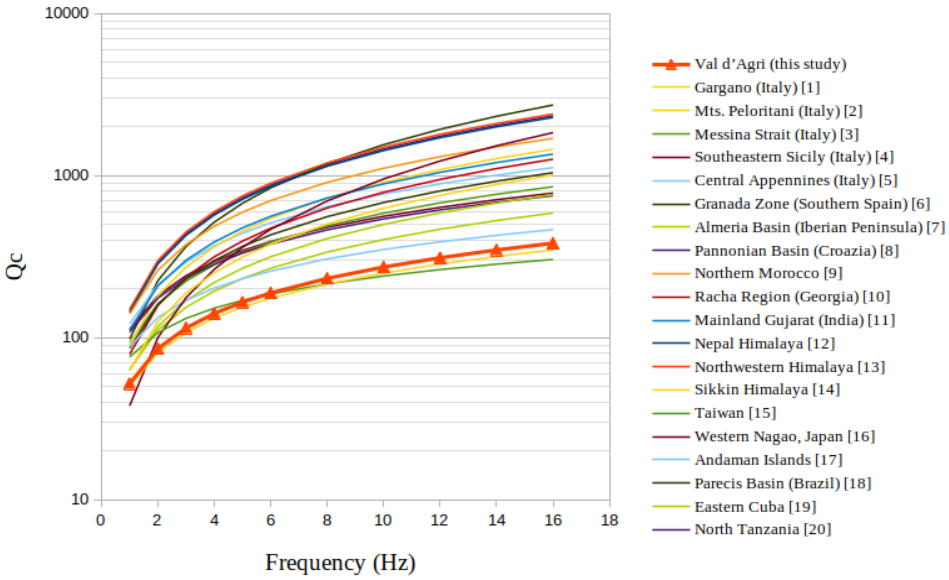

*Fig. 2 – Comparison between High Agri Valley Q_c (regression performed between 1.5*Ts and a lapse time of 30 s) and the same parameter obtained for other locations in the world.*

References

Bianco, F., Del Pezzo, E., Castellano, M., Ibanez, J., & Di Luccio, F. (2002). Separation of intrinsic and scattering seismic attenuation in the Southern Apennine zone, Italy. Geophysical Journal International, 150(1), 10-22.

Candela, S., Mazzoli, S., Megna, A., & Santini, S. (2015). Finite element modelling of stress field perturbations and interseismic crustal deformation in the Val d'Agri region, southern Apennines, Italy. Tectonophysics, 657, 245-259.

Filippucci, M., Lucente, S., Del Pezzo, E., de Lorenzo, S., Prosser, G., & Tallarico, A. (2021). 3D-Kernel Based Imaging of an Improved Estimation of (Qc) in the Northern Apulia (Southern Italy). Applied Sciences, 11(16), 7512.

Improta, L., Bagh, S., De Gori, P., Valoroso, L., Pastori, M., Piccinini, D., Chiarabba, C., Anselmi, M., Buttinelli, M. (2017). Reservoir structure and wastewater-induced seismicity at the Val d'Agri oilfield (Italy) shown by three-dimensional Vp and Vp/Vs local earthquake tomography. Journal of Geophysical Research: Solid Earth, 122.

Mayor, J., Calvet, M., Margerin, L. & Vanderhaeghe, O., 2016. Crustal structure of the Alps as seen by attenuation tomography, Earth planet. Sci. Lett., 439, 71–80

Patacca, E., & Scandone, P. (2007). Geology of the southern Apennines. Bollettino della Società Geologica Italiana, 7, 75-119.

Picozzi, M., Serlenga, V., Stabile, T.A. (2022). Spatio-temporal evolution of ground motion intensity caused by reservoir-induced seismicity at the Pertusillo artificial lake (southern Italy). Frontiers in Earth Science, 10, 1048196.

Sato H. (1977). Energy propagation including scattering effect: single isotropic scattering approximation. J. Phys. Earth, 25, pp. 27-41.

Stabile, T. A., Giocoli, A., Perrone, A., Piscitelli, S., & Lapenna, V. (2014). Fluid injection induced seismicity reveals a NE dipping fault in the southeastern sector of the High Agri Valley (southern Italy). Geophysical Research Letters, 41(16), 5847-5854.

Zolezzi, F., Morasca, P., Mayeda, K., Phillips, W. S., & Eva, C. (2008). Attenuation tomography of the southern Apennines (Italy). Journal of seismology, 12, 355-365.

Reference author: Salvatore Lucente, salvatore.lucente@uniba.it

MCMTpy waveform inversion package: testing a new method for moment tensor estimation

T. Mancuso[1], C. Totaro[1], B. Orecchio[1]

[1] Department of Mathematical and Computer Sciences, Physical and Earth Sciences (University of Messina, Italy)

Earthquake focal mechanism inversion is a seriously non-linear problem. It is well known that an accurate estimation of focal mechanisms is fundamental to obtain good constraints on regional stress field, to assess seismic hazard, and to better understand tectonic processes. The procedures commonly used to compute focal mechanism solutions are based on the polarity of P-wave first motion which may be biased by several factors (e.g., an inadequate coverage of seismic stations). Waveform inversion methods have so far demonstrated to be much more capable to furnish stable and reliable solutions (Presti et al., 2013), however needing a more accurate estimate of the associated errors which tend to be underestimated using linearized techniques (Scolaro et al., 2018). Bayesian inference is increasingly being applied to solve these non-linear problems because it has the advantage of quantifying uncertainties of parameters (Vasyura-Bathke et al., 2020).

In this work we present the application of a new Python package MCMTpy (Yin & Wang, 2022), which exploits the 'Cut-And-Paste' waveform inversion algorithm (CAP, Zhao & Helmberger, 1994; Zhu & Helmberger, 1996) and Bayesian inference, using Markov Chain to implement the source location and focal mechanism inversion in a unique workflow. The new approach can simultaneously invert for magnitude, focal mechanism, source location, source depth and origin time also providing a way to quantify uncertainties by statistical inference.

The main functions included in MCMTpy are source parameters inversion (i) under double-couple assumption with Markov-Chain Monte Carlo (MCMC) method, (ii) under double-couple assumption with a grid-search method and (iii) for the full moment tensor solution with MCMC method.

To test the robustness and limitations of the new package, we applied the MCMTpy to the 2016 M_w 6.0 Amatrice earthquake and to a smaller event (i.e., M_w 3.2) of the same sequence. We performed several tests by varying the starting solution, number of iterations, network geometry, and the type of computation (e.g., MCMC, grid-search method) and we compared our results with moment tensor solutions from other catalogues (e.g., Time Domain Moment Tensor). Test results were analysed in this study in order to evaluate reliability of moment tensor solutions and estimated uncertainties in different inversion settings.

References

Presti D., Billi A., Orecchio B., Totaro C., Faccenna C., Neri G.; 2013: Earthquake focal mechanisms, seismogenic stress, and seismotectonics of the Calabrian Arc, Italy. Tectonophysics, 602, 153–175, doi: 10.1016/j.tecto.2013.01.030.

Scolaro S., Totaro C., Presti D., D'Amico S., Neri G., Orecchio B.; 2018: Estimating Stability and Resolution of Waveform Inversion Focal Mechanisms. In Moment Tensor Solutions. Springer, 93–109, doi: 10.1007/978-3-319-77359-9_5.

Vasyura-Bathke H., Dettmer J., Steinberg A., Heimann S., Isken M. P., Zielke O., Mai P. M., Sudhaus H., Jónsson S.; 2020: The Bayesian earthquake analysis tool. Seismological Research Letters, 91 (2A): 1003–1018, doi: 10.1785/0220190075.

Yin F., Wang B.; 2022: MCMTpy: A Python Package for Source Parameters Inversion Based on Cut-and-Paste Algorithm and Markov Chain Monte Carlo. Seismological Research Letters, 93 (5): 2776–2792, doi: 10.1785/0220210336.

Zhao L. S., Helmberger D.; 1994: Source estimation from broad-band regional seismograms. Bulletin of the Seismological Society of America, 84 (1): 91–104.

Zhu L., Helmberger D.; 1996: Advancement in source estimation technique using broadband regional seismograms. Bulletin of the Seismological Society of America, 86 (5): 1634–1641.

Corresponding author: Thomas Mancuso - thomas.mancuso@studenti.unime.it

The gravitational signature of the dynamics of oceanization in the Gulf of Aden

A. M. Marotta[1], R. Barzaghi[2], A. Bollino[1], A. Regorda[1], R. Sabadini[1]

[1] *Department of Earth Sciences Ardito Desio, Universit`a degli Studi di Milano, Milano, Italy*
[2] *Department of Civil and Environmental Engineering, Politecnico di Milano, Milan, Italy*

We perform a new gravity analysis in the Gulf of Aden with the aim of finding new constraints on the geodynamic evolution of the area. Our analysis is developed within the frame of the recent GO_CONS_GCF_2_TIM_R6 global gravity model solution (Brockmann et al., 2021) that reflects the Earth's static gravity field as observed by GOCE (Gravity field and steady-state Ocean Circulation Explorer). We analyzed the solution at different harmonic degrees, to account for different depths and dimensions of the sources. Terrain correction has been performed by means of a spherical tesseroidal methodology (Marotta and Barzaghi, 2017) and the obtained corrected *Geodetic Residual Gravitation* has been compared to the *Model Residual Gravitation* predicted by means of a 2D visco-plastic finite element thermo-mechanic model that simulates the dynamics of the Gulf of Aden, from rifting to oceanization. In order to perform the comparison between observed and predicted gravitational features, data have been extracted along five profiles crossing the Gulf of Aden at different sectors, from the south-east to the north west. Via the *Model Residual Gravitation* we reproduce its geodetic counterpart, obtaining a characteristic hat-shaped pattern, with a central plateau portraying the highest values, flanked by two regions where the residual gravitation diminishes, finally reaching the lowest values at the far continental domains. The maximum variations of the residual gravitation values, from ridge to continental domain, range between 280 and 420 *mGal* and the steepest decrease occurs over distances of 200 km for the thick crust model and of 100–150 km for the thin crust model. Finally, the comparison between *Geodetic* and *Model Residual Gravitation* allows to further constrain the dynamics of the Gulf of Aden oceanization occurring by a slow passive rift of a hot 150 km thick lithosphere characterized by an initial 40 km thick crust.

References

Brockmann, J.M., Schubert, T., Schuh, W.D., 2021. An improved model of the Earth's static gravity field solely derived from reprocessed GOCE data. Surv. Geophys. 42, 277–316. https://doi.org/10.1007/s10712-020-09626-0.

Marotta, A.M., Barzaghi, R., 2017. A new methodology to compute the gravitational contribution of a spherical tesseroid based on the analytical solution of a sector of a spherical zonal band. J. Geod. 91, 1207–1224. https://doi.org/10.1007/s00190- 017-1018-x. Surname N.; 20xx: Title. Journal.

Corresponding author: anna.maria.marotta@unimi.it

Geofluids as a possible unconventional tool for Seismic Hazard Assessment.

G.Martinelli[1], L.Pierotti[2], G.Facca[2], F.Gherardi[2]

1 INGV, Dept.Palermo, Palermo, Italy

2 CNR-IGG, Pisa, Italy

In recent decades, phenomenological methods known as Recognition of Earthquake-Prone Areas (REPA) were set up for identifying potential sites of powerful earthquakes. The information on potential earthquake sources provided by the REPA method is an essential part of the seismic hazard assessment methodology. For the first time, we combined global-scale information on the geographic occurrence of geofluids with global-scale information on earthquake occurrence, heat flow distribution, and S-wave dispersion, to gain insight into the evolution of local stress-strain fields. We focused on areas characterized by the occurrence of thermal waters and/or by the release of deep-seated gases, as traced by the isotope composition of associated helium. We noticed that the geographical distribution of these geofluids might serve as an indirect indicator of crustal permeability anomalies generated by crustal deformation procedures. This study proposes adding geofluids to the list of fundamental geological parameters to be considered in hazard assessment research.

Corresponding author: giovanni.martinelli15@gmail.com

Joint inversion of gravity and magnetic data of the Cornubian Batholith (South-West UK)

G. Maurizio[1], C. Braitenberg[1]

1. Department of Mathematics, Informatics and Geosciences (MIGe), University of Trieste, Trieste, Italy,

The Inversion of the gravity and magnetic potential fields is a useful method to detect and identify a concealed crustal body. Depending on its physical properties and geometry, the positive or negative anomalies in the gravity and magnetic fields are detectable with appropriate instrumentation. The grav-mag method is a powerful tool in mineral exploration, used in first instance due to the natural 2D coverage of the data acquisition. The combination of magnetic and gravity datasets guarantees reliability to the inversion results and increases the probability that the detected bodies are realistic geological elements, resolving the ambiguity problem of the single field inversion result (Sampietro et al., 2022; Maurizio et al., 2023).

The Cornubian Batholith is a large early Permian granitic body in the south-west peninsula in Great Britain and is the post-collisional result of the Variscan orogeny. It is placed on the peninsula extending in west-southwest direction off-shore and is composed by six main plutons outcropping and cutting the upper Paleozoic coverage (Willis-Richards and Jackson, 1989). The five on-land plutons have been individually studied and it has been observed that each one has a distinctive mineralogy (Simons et al. 2016). The Cornubian Batholith has an important mining history, since from Prehistoric period. The ore fields were imposed in three distinct stages referred to as pre-, syn-, and post-batholith stages, in relation to the emplacement of the Cornubian Batholith (Willis-Richards and Jackson, 1989). Most of the mineralization took part simultaneously with the formation of the batholith, while remaining mineralization occurred with the thermal and tectonic evolution of the region (Willis-Richards and Jackson, 1989). Active mines are still present and are operative. The main activity in the area involves kaolin extraction, but several studies have shown its potential for Tin, Lithium and Tungsten production (Romer and Kroner, 2016; Simons et al., 2017), and for the exploitation of geothermal energy (Beamish and Busby, 2016; Reinecker et al., 2021).

To perform the inversion, we use the jif3d framework (Moorkamp et al., 2011) which is a jupyter collection of scripts for joint inversion of different datasets, in this case gravity and magnetic field measurements. Inversion was performed considering variation of information (Moorkamp, 2022): this means that the algorithm searches a one-to-one relation between the investigated properties. The inversion minimizes the misfit between observed and calculated fields and reduces the variation of information. At the end we obtain a model with density and susceptibility values that fit the observations and show correspondence between the two properties.

We propose the first results about our new model of the Cornubian Batholith, evidencing not only the edges of the body, but also the density and susceptibility distribution along the peninsula. The Cornubian ore field is a perfect area for studying granite-related hydrothermal mineralization, and a better appreciation of the physical properties distribution may allow it to be used as a perfect case study in the analysis of areas with similar geologic history, also considering its future importance regarding the mining industry and the green material transition.

References:

Beamish, D., Busby, J. (2016) The Cornubian geothermal province: heat production and flow in SW England: estimates from boreholes and airborne gamma-ray measurements. Geotherm Energy 4, 4. https://doi.org/10.1186/s40517-016-0046-8

Maurizio, G., Braitenberg, C., Sampietro, D., & Capponi, M. (2023). A new lithospheric density and magnetic susceptibility model of Iran, starting from high-resolution seismic tomography. Journal of Geophysical Research: Solid Earth, 128, e2023JB027383. https://doi.org/10.1029/2023JB027383

Moorkamp, M., Heincke, B., Jegen, M., Roberts, A. W., Hobbs, R. W. (2011). A framework for 3-D joint inversion of MT, gravity and seismic refraction data, Geophysical Journal International, Volume 184, Issue 1, Pages 477–493. https://doi.org/10.1111/j.1365-246X.2010.04856.x

Moorkamp, M. (2022). Deciphering the state of the lower crust and upper mantle with multi-physics inversion. Geophysical Research Letters, 49, e2021GL096336. https://doi.org/10.1029/2021GL096336

Reinecker, J., Gutmanis, J., Foxford, A., Cotton, L., Dalby, C., Law, R. (2021). Geothermal exploration and reservoir modelling of the United Downs deep geothermal project, Cornwall (UK), Geothermics, Volume 97, 102226, ISSN 0375-6505. https://doi.org/10.1016/j.geothermics.2021.102226.

Romer, R. L., Kroner, U. (2016). Phanerozoic tin and tungsten mineralization—Tectonic controls on the distribution of enriched protoliths and heat sources for crustal melting, Gondwana Research, Volume 31, Pages 60-95, ISSN 1342-937X. https://doi.org/10.1016/j.gr.2015.11.002.

Sampietro, D., Capponi, M., & Maurizio, G. (2022). 3D Bayesian inversion of potential fields: The Quebec Oka carbonatite complex case study. Geosciences, 12(10), 382. https://doi.org/10.3390/geosciences12100382

Simons, B., Shail, R. K., Andersen, J. C. Ø. (2016). The petrogenesis of the Early Permian Variscan granites of the Cornubian Batholith: Lower plate post-collisional peraluminous magmatism in the Rhenohercynian Zone of SW England, Lithos, Volume 260, Pages 76-94, ISSN 0024-4937. https://doi.org/10.1016/j.lithos.2016.05.010.

Simons, B., Andersen, J. C. Ø., Shail, R. K., Jenner, F. E. (2017). Fractionation of Li, Be, Ga, Nb, Ta, In, Sn, Sb, W and Bi in the peraluminous Early Permian Variscan granites of the Cornubian Batholith: Precursor processes to magmatic-hydrothermal mineralisation, Lithos, Volumes 278–281, Pages 491-512, ISSN 0024-4937. https://doi.org/10.1016/j.lithos.2017.02.007.

Willis-Richards, J., Jackson, N. J. (1989). Evolution of the Cornubian ore field, Southwest England; Part I, Batholith modeling and ore distribution. Economic Geology; 84 (5): 1078–1100. https://doi.org/10.2113/gsecongeo.84.5.1078

Upper Mantle structure below the Western Alps from P and S receiver functions

S. Monna [(1)], C. Montuori [(1)], F. Frugoni [(1)], C. Piromallo [(1)], L. Vinnik [(2)] and AlpArray Working Group

(1) Istituto Nazionale di Geofisica e Vulcanologia, Rome. Italy
(2) Institute of Physics of the Earth, Moscow. Russia

In spite of numerous active and passive seismological investigations on the Alpine orogen, many of the published observations focus on the Moho or the deeper part of the mantle, while reliable information on the LAB below the Alps is scarce.

We investigated the Moho and Lithosphere-Asthenosphere Boundary (LAB) for a broad region encompassing the Western Alps and including the Ivrea Geophysical Body (IGB), a fragment of mantle emplaced in the lower continental crust. After calculating a set of Receiver Function (RF) measurements from data recorded by the dense, broadband AlpArray Seismic Network, we produced seismic velocity profiles of the crust-uppermost mantle below each of the 50 analyzed stations down to about 250 km depth, through the joint inversion of P and S RFs. Lateral variations of the Moho and LAB topographies across the colliding plates, are constrained together with errors related to our measurements.

We considerably expand the published data of the Moho depth and add a unique set of new measurements of the LAB (Monna et al., 2022) and provide a contribution to the debate on the existence of continuous or interrupted continental subduction below the Western Alps. In fact, we find a comparable thickness (on average 90–100 km) of the Eurasia and Adria lithosphere, which are colliding below the IGB. Summarizing, Eurasia is not presently subducting below Adria with vertical continuity and there is a gap between the superficial (continental) European lithosphere and the deep (oceanic) lithosphere. These observations agree with the discontinuous structure of the Eurasia lithosphere imaged by some seismic tomography models (Fig. 1).

Corresponding authors: stephen.monna@ingv.it, caterina.montuori@ingv.it;

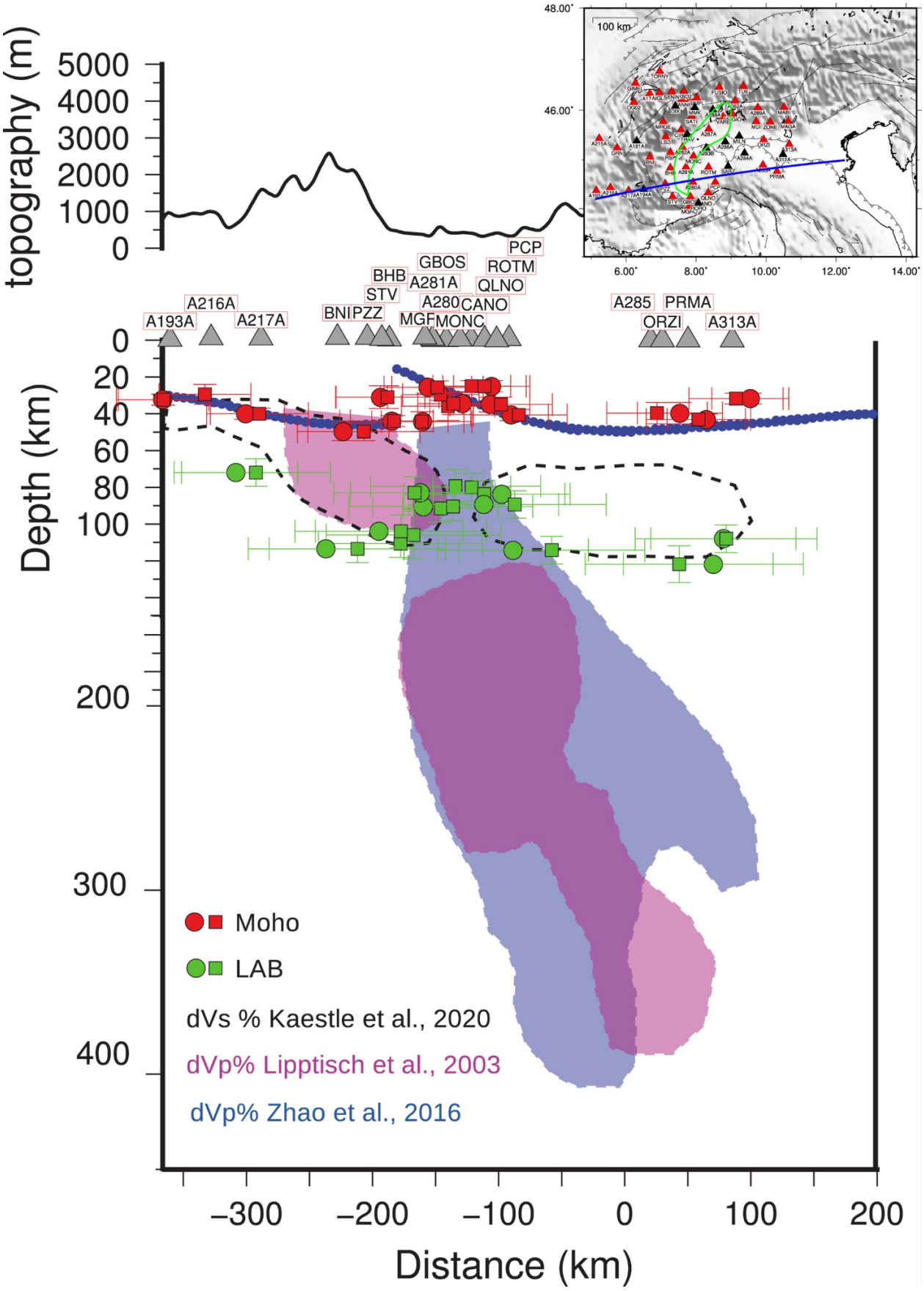

Figure 1- Moho (red symbols) and Lithosphere-Asthenosphere Boundary (LAB) (green symbols) depth for a profile shown in the inset. From Monna et al., 2022.

References

Monna, S., Montuori, C., Frugoni, F., Piromallo, C., Vinnik, L., & AlpArray Working Group (2022). Moho and LAB across the Western Alps (Europe) from P and S receiver function analysis. *Journal of Geophysical Research: Solid Earth*, 127, e2022JB025141. https://doi.org/10.1029/2022JB025141

Upper Mantle structure in the Tyrrhenian and Ionian basins (Central Mediterranean) from P and S receiver functions

C. Montuori [(1)], S. Monna [(1)], F. Frugoni [(1)], C. Piromallo [(1)], M. De Caro [(1)], A. Giuntini [(1)], G. Marinaro [(1)], V. Cormier [(2)] and L. Vinnik [(3)]

(1) Istituto Nazionale di Geofisica e Vulcanologia, Rome. Italy
(2) Dept. of Physics, University of Connecticut. USA
(3) Institute of Physics of the Earth, Moscow. Russia

We investigate the upper mantle discontinuities below the Tyrrhenian and Ionian basins by applying the P and S receiver function techniques to waveforms from broadband stations of the RSN network (Italy), located in Sicily, Ustica Island and Sardinia. These basins, with distinct characteristics in terms of age, origins, and crust-mantle structure, form part of the Central Mediterranean convective system. They are situated in different geological settings—the back-arc for the Tyrrhenian basin and the fore-arc for the Ionian basin—relative to the Calabrian slab. We model the 1D velocity structure below each station down to 250 km depth by joint inversion of P and S receiver functions through the Generalized Simulated Annealing method (Tsallis, 1988; Tsallis & Stariolo, 1996). Land-based observations are complemented with the analysis of data recorded by a broadband seismometer hosted on the NEMO-SN1 permanent observatory at 2100 m b.s.l (Western Ionian Regional Facility of EMSO ERIC, www.emso.eu). We show preliminary results for the Moho and Lithosphere-Asthenosphere-Boundary depth in the Ionian basin and integrate them with observations for the Tyrrhenian basin from our previous work (Monna et al., 2019).

We detect the mantle transition zone (MTZ) discontinuities (the '410' and '660') below the basins based on the receiver functions stacks and speculate on the origin of the observed MTZ thickness variations.

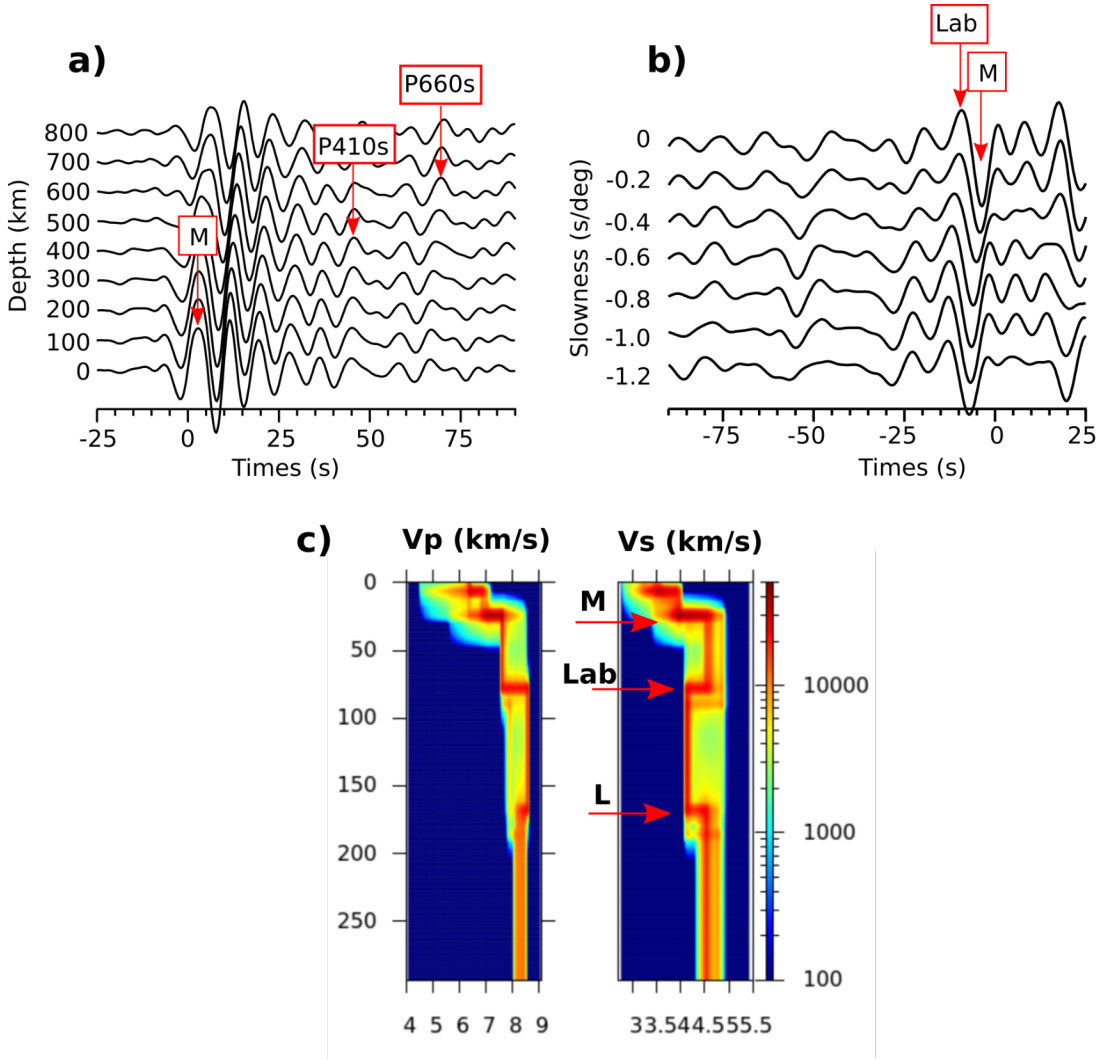

Fig. 1 – P (**a**) and S (**b**) receiver function stacks for a station located on the Hyblean Foreland (Sicily). **a**) Arrows indicate the positive phase converted at the Moho (M), at 410 km (P410s) and at 660 km depth (P660s). **b**) arrows indicate the negative phase converted at the Moho (M). Lab represents the positive candidate phase converted at the Lithosphere asthenosphere boundary. **c**) Vp and Vs velocity model obtained by joint inversion of P and S receiver functions. M: Moho; Lab: Lithosphere asthenosphere boundary; L: bottom of the asthenosphere.

References

Monna, S., Montuori, C., Piromallo, C., & Vinnik, L. (2019). Mantle structure in the central Mediterranean region from P and S receiver functions. Geochemistry, Geophysics, Geosystems, 20(10), 4545-4566. https://doi.org/10.1029/2019GC008496

Tsallis, C. (1988). Possible generalization of Boltzmann-Gibbs statistics. Journal of Statistical Physics, 52(1-2), 479-487. https://doi.org/10.1007/ bf01016429

Tsallis, C., & Stariolo, D. A. (1996). Generalized simulated Annealing. Physica A: Statistical Mechanics and its Applications, 233(1), 395-406. https://doi.org/10.1016/ s0378-4371(96)00271-3

Corresponding authors: caterina.montuori@ingv.it; stephen.monna@ingv.it

First evidence of water transport in the Earth's mantle from seismograms of Southern Tyrrhenian earthquakes

T. Ninivaggi[1], G. Selvaggi[2], S. Mazza[2], M. Filippucci2,[2,3], F. Tursi[4], W. Czuba[5]

[1] Istituto Nazionale di Geofisica e Vulcanologia, Sezione Irpinia, Grottaminarda, Italy
[2] Istituto Nazionale di Geofisica e Vulcanologia, ONT, Roma, Italy
[3] Dipartimento di Scienze della Terra e Geoambientali, Università degli Studi di Bari "Aldo Moro", Bari, Italy
[4] Dipartimento di Scienze della Terra, Università degli Studi di Torino, Torino, Italy
[5] Institute of Geophysics, Polish Academy of Sciences, Warsaw, Poland

Introduction

We have found a previously unreported later seismic phase in seismograms of European seismic stations from intermediate-depth and deep earthquakes of the Southern Tyrrhenian subduction system. We noticed the later phase on seismograms of a deep earthquake occurred in the Southern Tyrrhenian subduction region. The seismic phase, that we called the *x-phase*, appears few seconds after the direct *P*-wave, at stations located some hundreds of km away from the epicentre towards north (Fig. 1).
The interest in studying a later phase, detected after first arrivals, and observed in subduction zones, is motivated by the possibility to obtain indications on the slab properties (geometry, velocity anomalies, and petrology), because of their interaction with the subducting lithosphere. These later phases could be, for example, waves converted at the upper slab interface from the direct waves (e.g., Zhao et al., 1997) exploited to locate the upper boundary of the subducting plate. Later phases are also the depth phases, exploited to constrain hypocentral depths (e.g., Zhao, 2019). High frequency guided waves have been also interpreted as scattered seismic waves by heterogeneity in plate structure and enhanced by the presence of a metastable olivine wedge (Furumura et al., 2016).
As the *x-phase* is very likely linked to the subduction system, this research verifies the nature and the origin of the wave and gets new insights on the slab features.

Data and methods

To verify the robustness of the finding, we made a systematic analysis of the largest intermediate depth and deep earthquakes of the Southern Tyrrhenian subduction system, by selecting the 43 earthquakes occurred from 1990 to 2020 with magnitude ML ≥ 4.5 from the INGV Italian Seismological Instrumental and Parametric Database (http://cnt.rm.ingv.it/iside). The depth range is between 100 km and 644 km. The selected seismic stations are from 10° (central Africa) up to 71° North (Cape North in Norway) in latitude and between 10° (Portugal) West and 50° East (Mar Caspio) in longitude. We extracted and analysed about 25,000 digital waveforms from the

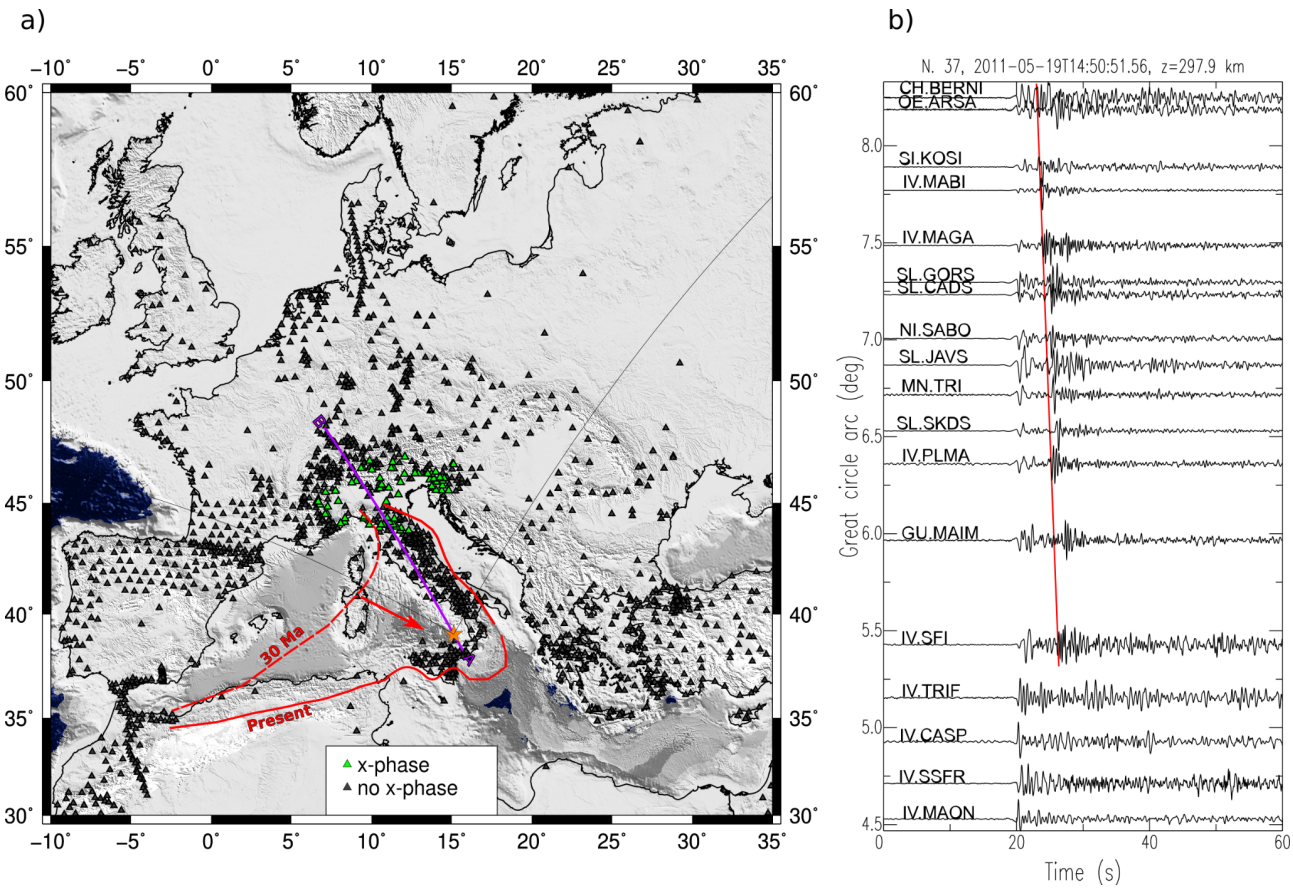

Fig. 1 – Observation of the later seismic phase. a) Stations which recorded the *x-phase* (green triangles). Seismograms of stations in black do not show the later arrival. Section trace AB of the Fig. 3, passing from the 2011 earthquake (n. 37). The red lines delineate the old (30 Ma) and the present subduction signature. The two thin black lines delineate the azimuths -60° and 30° starting from the epicentre. b) Time-distance vertical seismograms of the 2011 event aligned with P arrival time at 20 s. The red line marks the later phase arrivals.

European Integrated Data Archive, 2023 (EIDA, http://eida.ingv.it/) and from Incorporated Research Institutions for Seismology Data Management Centre, 2023 (IRIS DMC, https://service.iris.edu/).

We examined the seismological features of the wave to establish its nature by visual inspection of the waveforms and record sections. Later phases observed in a subduction context have characteristic features that allow to discern between the different type of waves interacting with the subducting lithosphere. We, therefore, compared the *x-phase* with seismic waves observed in subduction systems.

We finally reproduced its travel times and ray paths in a 2D velocity model with Seis83 software (Červený and Pšenčík, 1984) that makes use of ray-tracing technique (Červený et al., 1977). We used IASP91 velocity model (Kennett and Engdahl, 1991) to represent the velocity structure outside the slab. The slab boundaries were constrained by seismicity distribution of the Southern Tyrrhenian Sea, projected in the vertical section with trace AB in Figure 1a. According to tomographic studies (e.g., Amato et al., 1993; Scarfì et al., 2018), the subducting lithosphere is characterised by positive velocity anomalies. We increased the velocity inside the slab in different runs by a percentage between 1.5% and 5% to the IASP91 velocity values.

Results

The *x-phase* is prominent and easy to recognise. It often appears in the vertical and radial component as an impulsive arrival with a higher amplitude and frequency content than the first *P*-arrival. The *x-phase* shows a typical *P*-wave particle motion, and has an incidence angle always greater than the direct P. The travel time differences between the direct P wave and the *x-phase* decrease with increasing distances and with increasing depths of the earthquakes. The later phase has higher apparent velocities than P direct wave (about 11 km/s). These characteristics indicate that the *x-phase* is a compressional *P*-wave which leaves the source, travels downward, and interacts with an interface deeper than the hypocentre, in a less attenuating medium than the direct *P*-wave.

We observe this phase at stations from 6° to 9° from the epicentre, towards north (Fig. 2). Only seismograms of earthquakes located in a well-defined region of the slab, in the depth range of 215–320 km and below the eastern side of the Aeolian Arc, show the later *x-phase* (case 1 in Fig. 2). At greater distances, from 11° onwards, we found another arrival after the direct *P*-wave that is well reproduced by the 410 km discontinuity (P410P in the Fig. 2b, case 1 and 2). It is detected on earthquakes in the depth range of 200-400 km. Earthquakes deeper than 400 km, do not show neither of the two phases (case 3 in Fig. 2b).

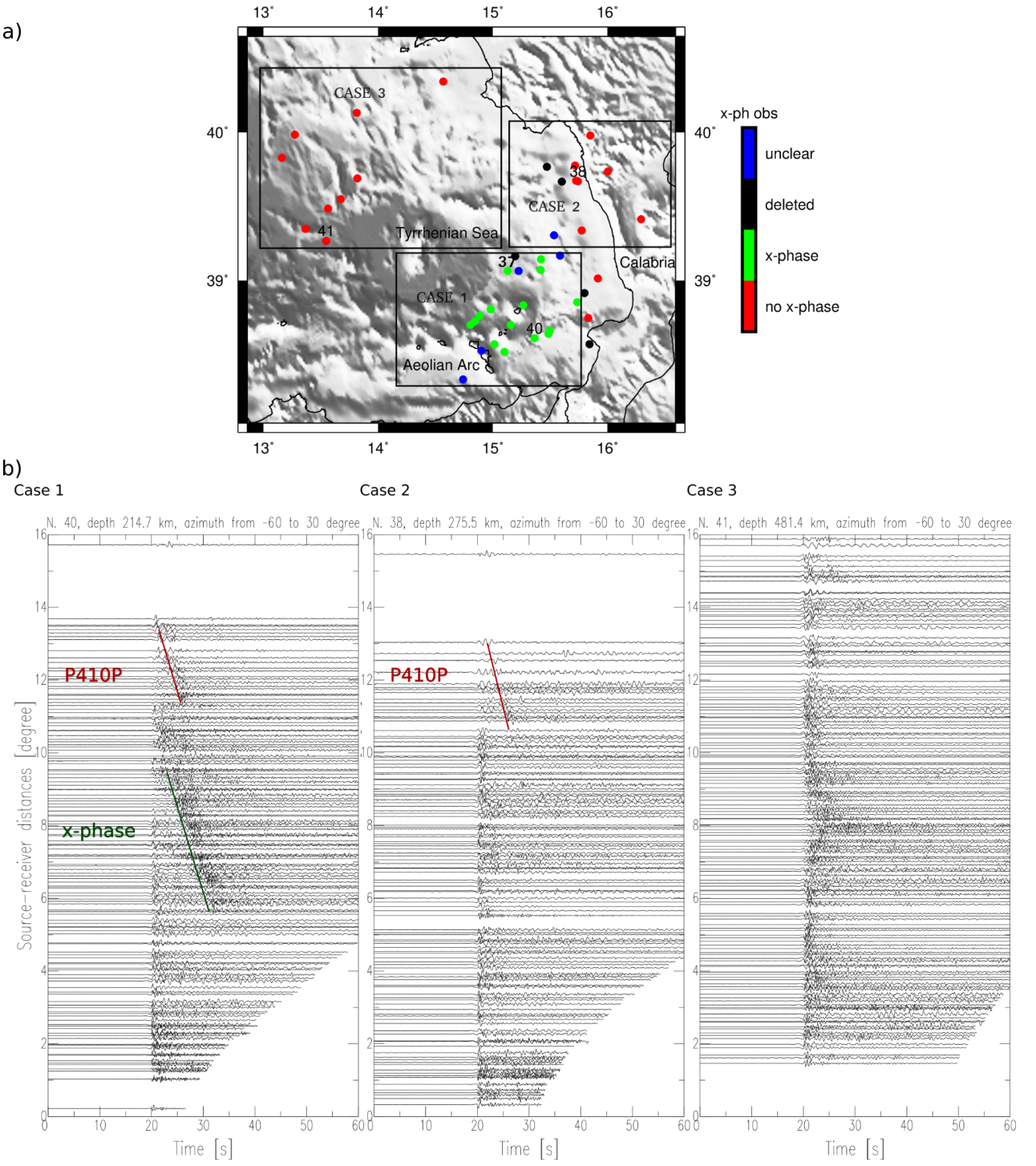

Fig. 2 – a) Map distribution of the earthquakes that show the later seismic phase (green dots), that do not show the *x-phase* (red dots) and those earthquakes where the presence of the *x-phase* is unclear (blue dots). Examples of record sections of the three cases we discuss in the text. The "N." in the title corresponds to number id in the map (N. 40, 38, 41). In the record section, each vertical waveform is normalised by its absolute maximum of amplitude, excluding *S*-waves from the plot and aligned by first arrival P, at 20 s. Waveforms are sorted by epicentral distances, shown on the vertical axis.

Arrival times indicate that the *x-phase* is not a depth phase, which shows an increasing difference of arrival time with the *P*-onset at increasing epicentral distances (Murphy and Barker, 2006). The *x-phase* is not even a *SP*-wave which is analysed by Zhao et al. (1997) for the Japan slab. It has an

apparent velocity almost equal or slightly smaller than the direct *P*-wave and the arrival time difference with the direct *P*-wave is constant. None of the main later phases associated to a subduction system and described in literature seems to be compatible with the seismological features found for the *x-phase*. The *x-phase* is a *P*-wave that propagates downward into the deepest portion of the subducted lithosphere below the Southern Tyrrhenian Sea.
The seismological constraints derived from the observations made in this work, allow us to design a simple 2D modelling by means of fitting the arrival times.
The arrivals of the direct *P*-wave are well fitted by a subducting lithosphere with an average increment of 1.5% of IASP91 velocity model, whereas the *x-phase* requires much faster velocities, at least 3% higher than IASP91 (Fig. 3a). Hence, we introduced a high velocity layer, HVL, in the region where we observe the hypocentre of the earthquakes with the later phase with an average increase of the velocity up to 3% with respect to IASP91. Following Pino and Helmberger (1997), the 410-km discontinuity is raised up to a depth of 370 km, as generally observed in subduction zones (Collier et al., 2001). The model can fit the arrival times of the x-phase for all the deep earthquakes below the Aeolian Island we have modelled (Fig. 3b-c). According to the final model, the *x-phase* is interpreted as a compressional wave that propagates downward in a "High Velocity Layer" (HVL) located in the subducted lithosphere and reflected from a shallower 410 km-discontinuity, located at 370 km of depth.

Discussion and conclusion

The 2D modelling states that a combination of velocity structure and geometric characteristics can reproduce rather well the *x-phase* observations and its travel times.
A 2D approach and a kinematic determination, however, is a first approximation to a more complex three-dimensional problem which need to be accompanied with a dynamic calculation in future research.
A HVL, as the one we have introduced in this work, has not been previously described from a seismological point of view. The tomographic images available for the Tyrrhenian subduction zone do not show such a HVL. However, the thickness of the HVL could be too narrow to be detected by the course grid used to model the mantle at those depths. The fact that we see the later *P*-arrival only in the Southern Tyrrhenian Subduction Zone, is probably due to the peculiar combination of the velocity structure, geometric conditions, and the station distribution in front of the slab.
Compressional velocities in the HVL between 250 and 370 km depth are from 8.9 to 9.15 km/s.
A simple explanation for the high velocity values of the HVL at those depths come from recent laboratory experiments on mineral transformations conducted at upper mantle conditions. The rocks that constitute the subducting lithosphere are locally hydrated with water incorporated into OH-bearing minerals (e.g., Hacker et al., 2003). One of the meta-stable minerals which compose the upper-mantle deep slabs is the dense magnesium hydrated silicate phase A. This mineral is considered the main responsible of the water transport into the deep Earth. Recent ultrasonic measurements of compressional waves on phase A in a cold subduction show an increase of *P*-velocities to the level introduced in the HVL model and at depths greater than 200 km (Cai et al., 2021). These depths are consistent with the range where we model the HVL in the Tyrrhenian subduction. Therefore, we interpret the HVL as related to the presence of the phase A, as inferred from laboratory experiments in cold subduction zones (van Keken et al., 2011; Cai et al., 2021), as the Tyrrhenian subduction seems to be. This is the first direct seismological observation of the phase A in the subduction process.

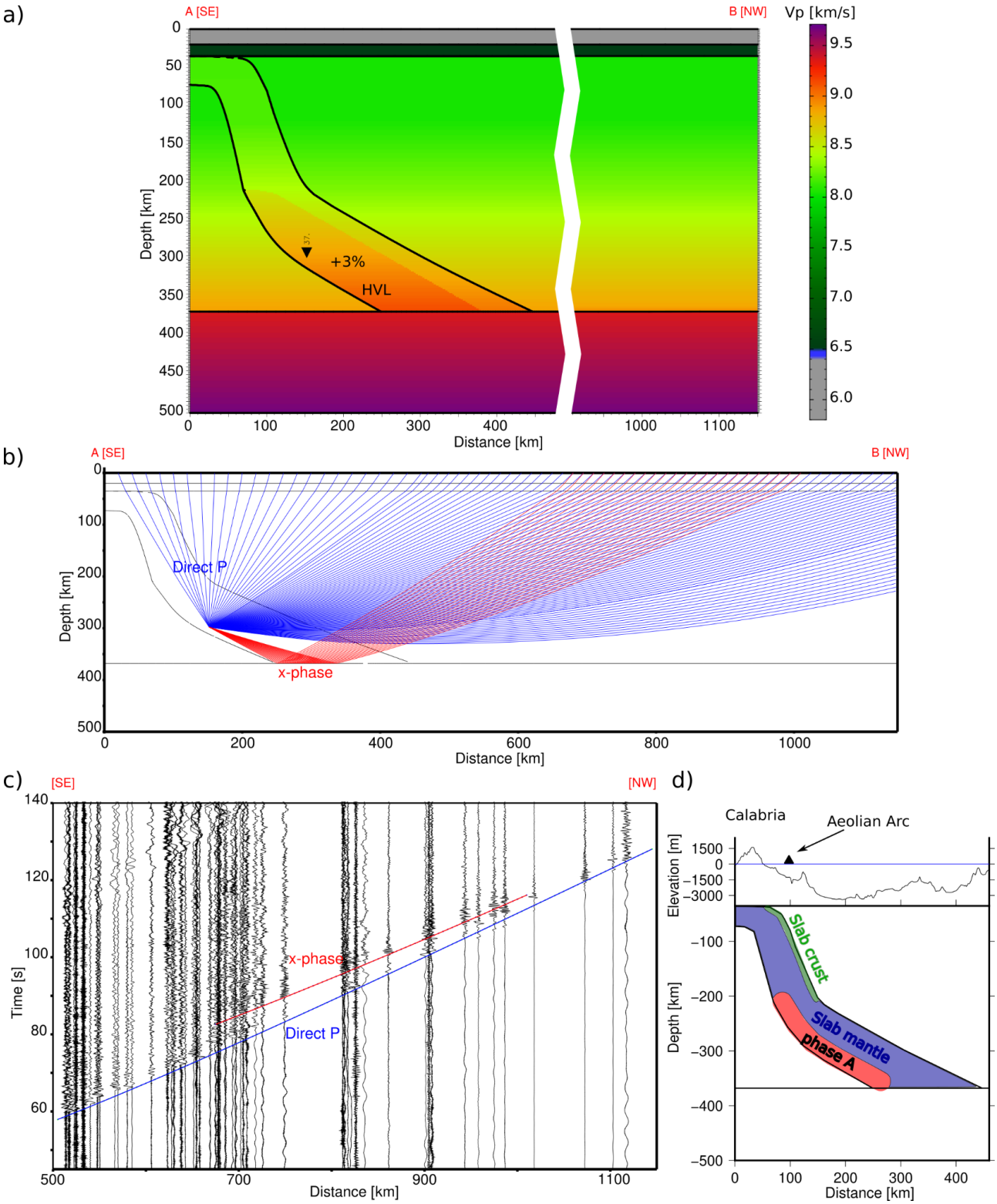

Fig. 3 (a) 2D velocity model, section trace AB in Fig. 1a (n.b. the section orientation is SE-NW to have increasing distances rightwards). The black triangle is the 2011 earthquake (N. 37) with *x-phase*; (b) Calculated ray paths for the earthquake N. 37; (c) calculated travel time curves on the observed record section of earthquake N. 37. The blue line shows the calculated direct P wave arrivals, and the red line is for the *x-phase*; (d) Sketch of the possible petrology and thickness of the HVL.

References

Amato, A., Alessandrini, B., Cimini, G., Frepoli, A., Selvaggi, G.; 1993: Active and remnant subducted slabs beneath Italy: evidence from seismic tomography and seismicity. Ann. Geophys. 36 (2) https://doi.org/10.4401/ag-4272.

Cai, N., Qi, X., Chen, T., Wang, S., Yu, T., Wang, Y., et al.; 2021: Enhanced visibility of subduction slabs by the formation of dense hydrous phase A. Geophys. Res. Lett. 48 (19), 1–10. https://doi.org/10.1029/2021GL095487.

Červený, V., Pšenčík, I.; 1984: SEIS83-Numerical modelling of seismic wave fields in 2-D laterally varying layered structures by the ray method. In: Engdahl, E.R. (Ed.), Documentation of Earthquake Algorithms, Report SE-35. World Data Center A for Solid Earth Geophysics, Boulder, pp. 36–40.

Červený, V., Molotkov, I.A., Pšenčík, I.; 1977: Ray method in seismology. Charles Univ. Press, Praha.

Collier, J.D., Helffrich, G.R., Wood, B.J.; 2001: Seismic discontinuities and subduction zones. Phys. Earth Planet. Inter. 127 (1–4), 35–49. https://doi.org/10.1016/S0031-9201(01)00220-5.

European Integrated Data Archive; 2023: http://eida.ingv.it/ (accessed 31 October 2021).

Furumura, T., Kennett, B.L.N., Padhy, S.; 2016: Enhanced waveguide effect for deep-focus earthquakes in the subducting Pacific slab produced by a metastable olivine wedge. J. Geophys. Res. Solid Earth 121, 6779–6796. https://doi.org/10.1002/2016JB013300.

Hacker, B.R., Abers, G.A., Peacock, S.M.; 2003: Subduction factory 1. Theoretical mineralogy, densities, seismic wave speeds, and H 2 O contents. J. Geophys. Res. Solid Earth 108 (B1), 1–26. https://doi.org/10.1029/2001jb001127.

ISIDe Working Group; 2007: Italian Seismological Instrumental and Parametric Database (ISIDe) [Dataset]. Istituto Nazionale di Geofisica e Vulcanologia (INGV). https://doi.Org/10.13127/ISIDE.

Incorporated Research Institutions for Seismology Data Management Centre; 2023: https://service.iris.edu/ (accessed 31 October 2021).

Kennett, B.L.N., Engdahl, E.R.; 1991: Traveltimes for global earthquake location and phase identification. Geophys. J. Int. 105, 429–465. https://doi.org/10.1111/j.1365-246X.1991.tb06724.x

Murphy, J.R., Barker, B.W.; 2006: Improved focal-depth determination through automated identification of the seismic depth phases pP and sP. Bull. Seismol. Soc. Am. 96 (4A), 1213–1229. https://doi.org/10.1785/0120050259.

Pino, N.A., Helmberger, D.V.; 1997: Upper mantle compressional velocity structure beneath the West Mediterranean Basin. J. Geophys. Res. 102 (B2), 2953–2967. https://doi.org/10.1029/96JB03461.

Scarfì, L., Barberi, G., Barreca, G., Cannavò, F., Koulakov, I., Patanè, D.; 2018: Slab narrowing in the Central Mediterranean: the Calabro-Ionian subduction zone as imaged by high resolution seismic tomography. Sci. Rep. 8 (1), 1–12. https://doi.org/10.1038/s41598.018-23543-8.

van Keken, P.E., Hacker, B.R., Syracuse, E.M., Abers, G.A.; 2011: Subduction factory: 4. Depth-dependent flux of H2O from subducting slabs worldwide. J. Geophys. Res. 116, B01401. https://doi.org/10.1029/2010JB007922.

Zhao, C.A.; 2019: Importance of later phases in seismic tomography. Phys. Earth Planet. Inter. 296, 106314 https://doi.org/10.1016/j.pepi.2019.106314.

Zhao, D., Matsuzawa, T., Hasegawa, A.; 1997: Morphology of the subducting slab boundary in the northeastern Japan arc. Phys. Earth Planet. Inter. 102 (1–2), 89–104. https://doi.org/10.1016/S0031-9201(96)03258-X.

Corresponding author: teresa.ninivaggi@ingv.it

Preliminary single-station template matching seismic catalogue for the area of Everest (Himalaya)

R Percacci[1], A Vuan[2], G Verza[3], M P Plasencia[2], D Sandron[2], F Pettenati[2]

1 Università degli studi di Trieste
2 Istituto di Oceanografia e di Geofisica Sperimentale, OGS, Trieste
3 EvK2cnr, Bergamo

From May 2014 to May 2023, we conducted a seismic monitoring project of the broadband station (IO.EVN), installed at the EvK2 Pyramid Laboratory/Observatory (Pettenati et al. 2014). The IO.EVN station, operated by OGS in the Everest region (Nepal) at an altitude of 5000 m above sea level. We applied the matched-filter method (Gibbons & Ringdal 2006; Vuan et al., 2018) to detect and locate seismic events within a 30 km radius from the station, using a catalogue of ~ 450 templates that we selected by a recursive STA/LTA trigger method based on a bandpass filter from 1 to 30 Hz and the coincidence of three channels. Single-station template matching is evaluated and improved by coupling the mutual information score and the cross-correlation values. We are currently analysing a rich catalogue of more than ~40000 events to distinguish between earthquakes, icequakes and rockfalls, and to identify any noise sources or artifacts related to the station operation or the surrounding environment.

References

Gibbons, S.J., Ringdal, F.; 2006: The detection of low magnitude seismic events using array-based waveform correlation. Geophys. J. Int. **165** (1), 149–166.

Pettenati F., C. Cravos, T. Dawa Sherpa, L. Adhikari Sherpa, M. P. Plasencia Linares, M. Romanelli, G. Verza; 2014: The installation of a new broadband seismometer to the EVK2-CNR Pyramid International Laboratory-Observatory (Everest, Nepal). 33° Convegno Nazionale Gruppo Nazionale di Geofisica della Terra Solida GNGTS. Bologna, 25-27 Novembre. 2014. Abstract.

Vuan A., Sugan M., Amati G., Kato A.; 2018: Improving the Detection of Low-Magnitude Seismicity Preceding the Mw 6.3 L'Aquila Earthquake: Development of a Scalable Code Based on the Cross Correlation of Template Earthquakes. *Bull Seismol Soc Am* 2018; **108** (1), 471–480. doi: https://doi.org/10.1785/0120170106

Space Weather: Central Italy Geoelectric-Field Mapping

G. Pignatiello[1], I. Coco[2], M. De Girolamo[2], F. Giannattasio[2], V. Materni[2], L. Miconi[2], G. Romano[1], V. Romano[2], V. Sapia[2], S. Tripaldi[1], R. Tozzi[2], A. Siniscalchi[1], P. De Michelis[2]

[1] Dipartimento di Scienze della Terra e Geoambientali, Università degli Studi di Bari, "Aldo Moro", Bari, Italy
[2] Istituto Nazionale di Geofisica e Vulcanologia, Roma, Italy

External dynamic processes related to extreme solar activity events can cause temporary disturbances of the Earth's magnetic field.

These geomagnetic disturbances induce geoelectric fields in the subsurface that generate low-frequency geomagnetically induced electric currents (GICs), which, flowing in metallic electrically conductive structures, can cause them to be damaged or malfunction.

Considering the sudden growth of the Sun's magnetic activity, which in the current solar cycle will peak in the year 2024, and the increasing dependence on electrical power and communication systems in our daily lives, many countries around the world are developing national strategies and risk assessment procedures for mitigating the risks associated with Space Weather events (A. Kelbert, 2020).

From the need to better understand the risk associated with the occurrence of GICs, the INGV research project called "MARGE", geoelectromagnetic risk mapping, was born. It aims to develop geoelectric field maps for real-time monitoring of ground effects related to Space Weather events as well as to define a 3D model of electrical resistivity at the regional scale of the middle crust and upper mantle of central Italy, so as to improve knowledge about the physical characteristics of the crust and mantle in the area under investigation.

This model will also be used for more accurate prediction of GICs.

This note will show the results of the analysis of simultaneous variable magnetic field recordings recorded in Central Italy observatories and electromagnetic field with broadband magnetotelluric stations at a distance of a few hundred km with a threefold purpose:

1. to estimate the transfer function for the magnetotelluric site for periods characterized by low Dst;
2. compare the electric field measured at periods with high Dst and compare it with that predicted by the magnetic field of the magnetic observatory in the same periods;
3. compare the transfer function at the site during periods of low Dst with that of high Dst.

References

Kelbert, A. (2020). The role of global/regional Earth conductivity models in natural geomagnetic hazard mitigation. Surveys in Geophysics,41, 115–166.https://doi.org/10.1007/s10712-019-09579-z

Corresponding author: Giulia Pignatiello (giulia.pignatiello@uniba.it)

Moment tensor inversion of the 1947 Squillace Basin earthquake (Southern Italy) using digitized analog seismograms

S. Scolaro[1*], J. Batlló[2], B. Orecchio[1], D. Presti[1], D. Stich[3], C. Totaro[1]

1.Department of Mathematics, Computer Sciences, Physics, and Earth Sciences, University of Messina, Italy
2.Institut Cartogràfic i Geològic de Catalunya, Barcelona, Spain;
3.Instituto Andaluz de Geofísica, Universidad de Granada, Spain

The importance of historical seismic data legacy has amplified within the scientific community due to its potential synergy with modern analysis techniques. Seismograms from the analog recording era cover more than a century of seismic activity, providing significant contributions especially in studying regions affected by major historical seismic events and minor activity in recent decades. We collected and digitized analog seismograms to investigate the 11 May 1947 earthquake that is, according to the CPTI15 catalog (Rovida et al., 2022), the largest seismic event (proxy Mw 5.7) instrumentally recorded in the Squillace Basin, at the Ionian offshore of central Calabria. This sector is a high seismic risk area framed in the complex geodynamic setting leaded by the NW-trending Nubia-Eurasia convergence and the southeastward Ionian slab rollback. Moreover, the presence of the lateral edge of the Ionian slab has been suggested and an intense debate is still open concerning the possible existence and the proper location of a Subduction-Transform Edge Propagator (STEP) fault zone.

Through a time-domain waveform inversion algorithm specifically developed for waveform inversion of analog seismograms (Stich et al., 2005) we computed the first moment tensor solution for the 1947 earthquake. Station bulletins and original seismograms recorded by medium-to-long-period seismographs have been collected, digitized and properly corrected for geometrical distortions. The moment tensor solution obtained for the 1947 earthquake indicates a strike-slip mechanism, focal depth of 28 km and Mw 5.1, that represents the first moment magnitude estimate directly computed from waveform analysis. The result has been accurately checked by performing several inversion tests and interpreted in the frame of the regional seismotectonic scenario (Orecchio et al., 2021 and references therein), where the obtained left-lateral kinematics on about WNW-ESE oriented fault are compatible with a STEP fault activity in the Squillace Basin area.

Our study demonstrates the invaluable and irreplaceable role of information derived from pre-digital seismograms in providing new constraints for local and regional seismotectonic modeling in high seismic risk regions like the Calabrian Arc. Furthermore, the presented analysis is also useful for sharing within the scientific community some methodological challenges linked to the management of historical seismograms.

References

Orecchio B., Scolaro S., Batlló J., Neri G., Presti D., Stich D., and Totaro C., (2021). New Results for the 1968 Belice, South Italy, Seismic Sequence: Solving the Long-Lasting Ambiguity on Causative Source, Seismol. Res. Lett., 92(4), 2364-2381. Doi:10.1785/0220200277

Rovida A., Locati M., Camassi R., Lolli B., Gasperini P., and Antonucci A. (2022). Italian Parametric Earthquake Catalogue (CPTI15), version 4.0. Istituto Nazionale di Geofisica e Vulcanologia (INGV). doi:10.13127/CPTI/CPTI15.4

Stich D., Batlló J., Macià R., Teves-Costa P., and Morales J. (2005). Moment tensor inversion with single-component historical seismograms: The 1909 Benavente (Portugal) and Lambesc (France) earthquakes, Geophys. J. Int., 162(3), 850–858. Doi: 10.1111/j.1365-246X.2005.02680.x

Corresponding author: silscolaro@unime.it

Thermo-poro-elastic modeling of the inflation phase during the 2021 Vulcano Island (Italy) unrest

S. C. Stissi[1], G. Currenti[1], F. Cannavò[1], R. Napoli[1]

[1] *Istituto Nazionale di Geofisica e Vulcanologia (Catania, Italy)*

Starting from September 2021, Vulcano Island has been affected by an unrest episode, characterised by the increase in gas emission, seismic activity, and edifice inflation (Aiuppa et al., 2022; Federico et al., 2023). The continuous and stable radial expansion of the volcano edifice continuing until mid-October 2021, that affected the GPS stations closer to the summit crater, suggested a deformation source located below La Fossa crater. The temporal evolution of the deformation pattern is indicative of a spatially stationary source. The deformation pattern and the lack of shallow VT seismicity ruled out a possible involvement of shallow magmatic intrusion. Therefore, it is likely that the observed displacements have been generated by the thermo-poro-elastic response of the rocks to the increase of hot fluid flow at shallow depth originating from the degassing of a deeper magma source.

With this in mind, we review and develop (semi-)analytical formulations to calculate the ground deformation induced by homogeneous distributions of pore-pressure and/or temperature changes within thermo-poro-elastic sources with simple geometries, embedded in an elastic, isotropic and homogeneous half-space. We investigate two models: spherical (Davies, 2003; Rinaldi et al., 2011) and cylindrical.

For homogeneous and isotropic distributions of rock elastic parameters and irrotational displacement fields, the deformations related to hydrothermal activity are given by the gradient of a potential that obeys a Poisson equation, establishing a mathematical analogy between displacement and gravitational problems in an infinite space (Wang, 2000). The semi-analytic formulation for the cylindrical source is derived as a function of this analogy starting from the solution to calculate the gravity changes due to homogeneous distributions of the density variations (Hemmings et al., 2016).

After checking the correctness of the developed thermo-poro-elastic displacement formulations through a comparison with the finite-element solutions (COMSOL, 2012), we verify whether the amplitude and extent of the deformation recorded on Vulcano Island from September to mid-October 2021 are consistent with a thermo-poro-elastic response of the rock, applying both models (sphere and cylinder) in the inversion of the GPS daily monitoring data. The inversion results have suggested a deformation source located below La Fossa crater at a depth of approximately 800 m from the ground surface undergoing a volume change of approximately 10^5 m^3(Stissi et al., 2023). The modeling results support the hypothesis that the observed deformation on the Island are induced by the circulation of fluids (Figure 1), fed by the degassing of a deeper magmatic system (Aiuppa et al., 2022; Federico et al., 2023) without necessarily invoking the migration of magma to shallow levels. We assume that a growing magmatic fluid input can explain both the source inflation and the simultaneous increase in gas emission from September to mid-October 2021. In particular, both, the fast deformation rate and the gas discharge, support the hypothesis that the inflation was engendered by the disequilibrium between the magmatic fluids entering the hydrothermal system and the hydrothermal-magmatic fluids released at the surface. Therefore, at the onset of the 2021 unrest, hot magmatic fluids raised from the deeper magmatic system, have reached the hydrothermal system at a shallower depth where they have generated a local overpressure, which produced the symmetric inflation pattern centred in the La Fossa crater. The stop in the increase in deformation starting from mid-October, and the continued gas emission at a level above the background, can be interpreted as a change in the response of the porous medium. Indeed, the interaction between rocks and fluid could have altered the permeability, the increase of which has favoured the fluid release and has hindered a further increase in pore-pressure.

Based on the observations and the obtained results, we can state that, despite the introduced simplifications, the derived thermo-poro-elastic solutions can provide a first-order approximation of ground displacements and source parameters. Therefore, they represent an excellent method for a first interpretation of geodetic data during unrest periods and for a better understanding of the evolution of the hydrothermal systems, contributing to the hazard assessment during volcanic crises.

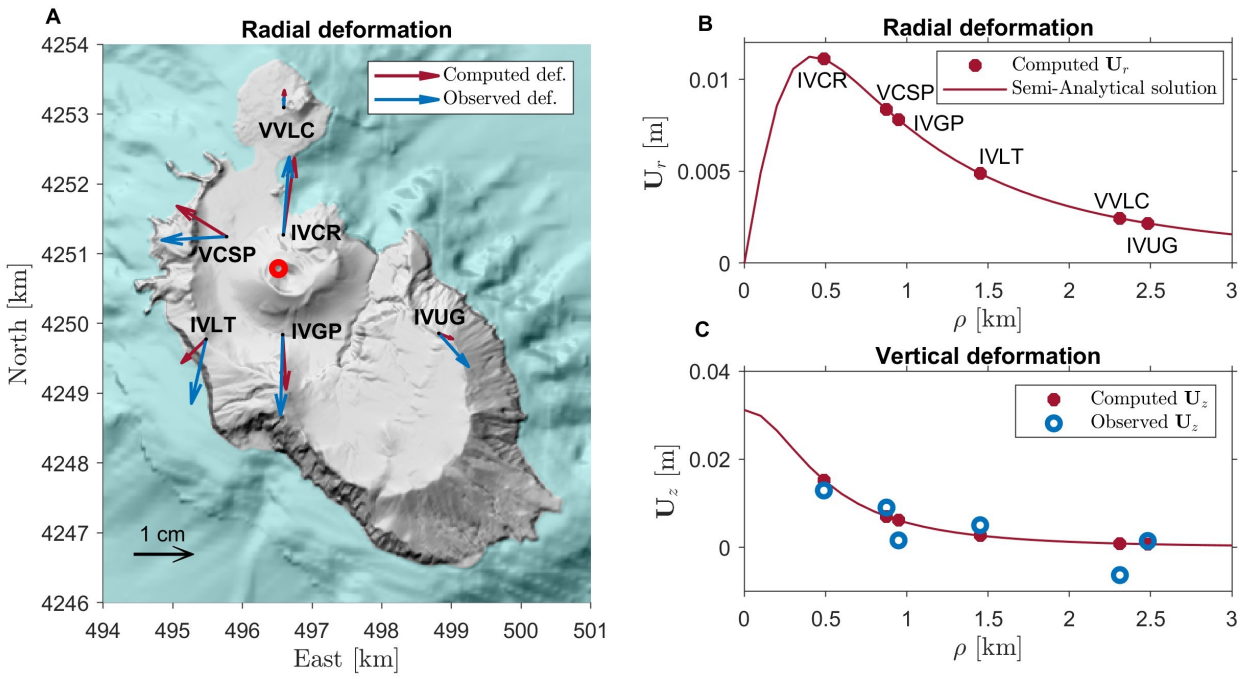

Figure 1: Comparison between observed and optimum computed deformation for the cylindrical source. **(A)** U_x and U_y components of the radial deformation in each monitoring station; the red circle indicates the position of the source. **(B)** Radial deformation U_r as a function of the radial distance ρ of the stations from the deformation source centre. **(C)** Vertical deformation U_z as a function of the radial distance ρ of the stations from the source centre.

References

Davies J. H.; 2003: Elastic field in a semi-infinite solid due to thermal expansion or a coherently misfitting inclusion. J. Appl. Mech. 70 (5), 655–660.

Federico C., Cocina O., Gambino S., Paonita A., Branca S., Coltelli M., Italiano F., Bruno V., Caltabiano T., Camarda M., Capasso G., De Gregorio S., Diliberto I. S., Di Martino R. M. R., Falsaperla S., Greco F., Pecoraino G., Salerno G., Sciotto M., Bellomo S., Di Grazia G., Ferrari F., Gattuso A., La Pica L., Mattia M., Pisciotta A. F., Pruiti L., Sortino F.; 2023: Inferences on the 2021 ongoing volcanic unrest at vulcano island (Italy) through a comprehensive multidisciplinary surveillance network. Remote Sens. 15, 1405.

Hemmings B., Gottsmann J., Whitaker F., Coco A.; 2016: Investigating hydrological contributions to volcano monitoring signals: A time-lapse gravity example. Geophys. J. Int. 207 (1), 259–273.

Rinaldi A. P., Todesco M., Vandemeulebrouck J., Revil A., Bonafede M.; 2011: Electrical conductivity, ground displacement, gravity changes, and gas flow at solfatara crater (Campi Flegrei caldera, Italy): results from numerical modeling. J. Volcanol. Geother. Res. 207 (3-4), 93–105.

Stissi S. C., Napoli R., Currenti G., Afanasyev A., Montegrossi G.; 2021: Influence of permeability on the hydrothermal system at Vulcano Island (Italy): inferences from numerical simulations. Earth, Planets Space 73, 179.

Stissi S. C., Currenti G., Cannavò F., Napoli, R.; 2023: Evidence of poro-elastic inflation at the onset of the 2021 Vulcano Island (Italy) unrest. Front Earth Sci 11:1179095.

Wang H. F.; 2000: Theory of linear poroelasticity with Applications to Geomechanics and hydrogeology. Princeton University Press.

Santina Chiara Stissi: santina.stissi@ingv.it

The Attenuation and Scattering Signature of Fluid Reservoirs and Tectonic Interactions in the Central-Southern Apennines (Italy)

D. Talone*[1,2], L. De Siena[2,3], G. Lavecchia[1,2], R. de Nardis[1,2]

[1]Department of Psychological Sciences, Health and Territory, University of the Studies "G. d'Annunzio", Chieti, Italy

[2]CRUST-Interuniversity Center for 3D Seismotectonics with Territorial Applications, Chieti, Italy

[3]Dipartimento di Fisica e Astronomia (DIFA), Alma Mater Studiorum-Università di Bologna, Bologna, Italy

For decades, seismic tomography techniques have imaged the Italian peninsula (Di Stefano and Ciaccio, 2014; Gualtieri et al., 2014; Scafidi et al., 2009; Zhao et al., 2016). Both large-scale and very local models have been produced, especially for the Northern and the Southern Apennines. Despite its seismotectonic interest, no seismic crustal image of the Central-Southern Apennines transition zone is currently available**,** primarily due to its low rates of seismic activity (Bagh et al., 2007; Frepoli et al., 2017; Romano et al., 2013; Trionfera et al., 2019).

Nowadays, the improvements in seismic detection infrastructures' sensibility and coverage allow the enrichment of seismic databases and the possibility of reliable geophysical imaging in these poor conditions. We applied the MuRAT package (De Siena et al., 2014; De Siena et al., 2014; Reiss et al., 2022) to perform 3D attenuation and scattering tomography, using seismic amplitudes from earthquake recordings to measure and model the total and scattering energy lost by P- and S-waves while propagating through space. The technique has been applied to volcanic contexts and tectonic frameworks showing high sensitivity to fluid-driven processes and strain accumulation (Amoroso et al., 2017; Di Martino et al., 2022; King et al., 2023, 2022; Sketsiou et al., 2021; Tisato and Quintal, 2014). Fracture networks and their potential fluid storage are thus ideal targets for these tomographic studies. By analyzing the peak delay of seismic envelopes and the coda-normalized energy loss, we interpreted the novel 3D models as images of the principal tectonic structures and fluid pathways.

The most relevant feature in the area is a high attenuation and scattering anomalies corresponding to almost the entire Apenninic Chain and related to its East- and West-dipping extensional Quaternary tectonic alignments. The fracture zones associated with the principal faults represent preferential ways for the circulation of CO^2-bearing fluids. A deep, wide, high-attenuation and high-scattering anomaly below the Matese extensional system appears the likely source of fluids feeding springs at its surface, while a smaller anomaly, at about 7 km depths, can be located in the proximity of the L'Aquila 2009 seismogenic area. The two attenuative areas are divided by a low attenuation and scattering volume acting as barriers for fluids and earthquake propagation. This detects a locked seismic zone with low seismic energy release corresponding to the Fucino and Morrone-Porrara fault systems and representing an area of stress accumulation and significant seismic hazard.

Amoroso, O., Russo, G., De Landro, G., Zollo, A., Garambois, S., Mazzoli, S., Parente, M., Virieux, J., 2017. From velocity and attenuation tomography to rock physical modeling: Inferences on fluid-driven earthquake processes at the Irpinia fault system in southern Italy: From Seismic Tomography to Rock Modeling. Geophys. Res. Lett. 44, 6752–6760. https://doi.org/10.1002/2016GL072346

Bagh, S., Chiaraluce, L., De Gori, P., Moretti, M., Govoni, A., Chiarabba, C., Di Bartolomeo, P., Romanelli, M., 2007. Background seismicity in the Central Apennines of Italy: The Abruzzo region case study. Tectonophysics 444, 80–92. https://doi.org/10.1016/j.tecto.2007.08.009

De Siena, L., Thomas, C., Aster, R., 2014. Multi-scale reasonable attenuation tomography analysis (MuRAT): An imaging algorithm designed for volcanic regions. Journal of Volcanology and Geothermal Research 277, 22–35. https://doi.org/10.1016/j.jvolgeores.2014.03.009

De Siena, L., Thomas, C., Waite, G.P., Moran, S.C., Klemme, S., 2014. Attenuation and scattering tomography of the deep plumbing system of Mount St. Helens. J. Geophys. Res. Solid Earth 119, 8223–8238. https://doi.org/10.1002/2014JB011372

Di Martino, M.D.P., De Siena, L., Tisato, N., 2022. Pore Space Topology Controls Ultrasonic Waveforms in Dry Volcanic Rocks. Geophysical Research Letters 49. https://doi.org/10.1029/2022GL100310

Di Stefano, R., Ciaccio, M.G., 2014. The lithosphere and asthenosphere system in Italy as inferred from the Vp and Vs 3D velocity model and Moho map. Journal of Geodynamics 82, 16–25. https://doi.org/10.1016/j.jog.2014.09.006

Frepoli, A., Cimini, G.B., De Gori, P., De Luca, G., Marchetti, A., Monna, S., Montuori, C., Pagliuca, N.M., 2017. Seismic sequences and swarms in the Latium-Abruzzo-Molise Apennines (central Italy): New observations and analysis from a dense monitoring of the recent activity. Tectonophysics 712–713, 312–329. https://doi.org/10.1016/j.tecto.2017.05.026

Gualtieri, L., Serretti, P., Morelli, A., 2014. Finite-difference P wave travel time seismic tomography of the crust and uppermost mantle in the Italian region: P WAVE TOMOGRAPHY OF THE ITALIAN REGION. Geochem. Geophys. Geosyst. 15, 69–88. https://doi.org/10.1002/2013GC004988

King, T., De Siena, L., Benson, P., Vinciguerra, S., 2022. Mapping faults in the laboratory with seismic scattering 1: the laboratory perspective. Geophysical Journal International 232, 1590–1599. https://doi.org/10.1093/gji/ggac409

King, T., De Siena, L., Zhang, Y., Nakata, N., Benson, P., Vinciguerra, S., 2023. Mapping faults in the laboratory with seismic scattering 2: the modelling perspective. Geophysical Journal International 234, 1024–1031. https://doi.org/10.1093/gji/ggad100

Reiss, M.C., De Siena, L., Muirhead, J.D., 2022. The Interconnected Magmatic Plumbing System of the Natron Rift. Geophysical Research Letters 49. https://doi.org/10.1029/2022GL098922

Romano, M.A., de Nardis, R., Garbin, M., Peruzza, L., Priolo, E., Lavecchia, G., Romanelli, M., 2013. Temporary seismic monitoring of the Sulmona area (Abruzzo, Italy): a quality study of microearthquake locations. Nat. Hazards Earth Syst. Sci. 13, 2727–2744. https://doi.org/10.5194/nhess-13-2727-2013

Scafidi, D., Solarino, S., Eva, C., 2009. P wave seismic velocity and Vp/Vs ratio beneath the Italian peninsula from local earthquake tomography. Tectonophysics 465, 1–23. https://doi.org/10.1016/j.tecto.2008.07.013

Sketsiou, P., De Siena, L., Gabrielli, S., Napolitano, F., 2021. 3-D attenuation image of fluid storage and tectonic interactions across the Pollino fault network. Geophysical Journal International 226, 536–547. https://doi.org/10.1093/gji/ggab109

Tisato, N., Quintal, B., 2014. Laboratory measurements of seismic attenuation in sandstone: Strain versus fluid saturation effects. GEOPHYSICS 79, WB9–WB14. https://doi.org/10.1190/geo2013-0419.1

Trionfera, B., Frepoli, A., De Luca, G., De Gori, P., Doglioni, C., 2019. The 2013–2018 Matese and Beneventano Seismic Sequences (Central–Southern Apennines): New Constraints on the Hypocentral Depth Determination. Geosciences 10, 17. https://doi.org/10.3390/geosciences10010017

Zhao, L., Paul, A., Malusà, M.G., Xu, X., Zheng, T., Solarino, S., Guillot, S., Schwartz, S., Dumont, T., Salimbeni, S., Aubert, C., Pondrelli, S., Wang, Q., Zhu, R., 2016. Continuity of the Alpine slab unraveled by high-resolution P wave tomography: Continuity of the Alpine Slab. J. Geophys. Res. Solid Earth 121, 8720–8737. https://doi.org/10.1002/2016JB013310

* **Reference author:** Talone Donato, donato.talone@unich.it

Twenty years of geodetic monitoring in NE-Italy

L. Tunini[1], A. Magrin[1], D. Zuliani[1], G. Rossi[1]

[1]National Institute of Oceanography and Applied Geophysics - OGS - Italy

North-Eastern Italy is part of the diffused tectonic boundary that accommodates the present-day convergence between the Adria microplate and the Eurasia plate. It is a region characterized by low deformation rates and moderate seismicity. It greatly benefits from continuous and high-precision geodetic monitoring, since it has been equipped with a permanent GNSS network providing real-time data and daily observations over two decades. This network, called Friuli Regional Deformation Network FReDNet (https://frednet.crs.ogs.it), has been established by the National Institute of Oceanography and Applied Geophysics - OGS with the aim of monitoring the distribution of crustal deformation and providing supplementary information for the regional earthquake hazard assessment (Zuliani et al., 2018). From the first stations installed in 2002, FReDNet has been continuously growing until counting, nowadays, 22 permanent GNSS stations covering homogeneously the eastern Alps, the alluvial plain, and the coastal areas of NE-Italy. Most of the time series are longer than 15 years.

Data from FReDNet are collected, quality-checked, transformed into RINEX-formatted files, and then released under a Creative Common license (CC BY-SA) along with their metadata, through a public ftp repository (FReDNet DC 2016), accessible at the link https://frednet.crs.ogs.it/DOI/.

We processed daily GNSS data from FReDNet and from other permanent networks, using the GAMIT/GLOBK software package version 10.71 (Herring et al., 2018). Data processing was performed on the HPC cluster GALILEO100 of CINECA, which uses the SLURM system for job scheduling and workload management (Tunini et al., 2023).

Here, we present the processing results focused on the NE-Italy, in terms of time-series and velocity field, and we illustrate the different aspects considered to test the reliability of the adopted processing procedure and of the obtained results, such as considering or avoiding tidal or non-tidal loadings or changing the reference stations, the influence of the type of GNSS monuments, or the location of the geodetic antenna (on a roof or in the free-field).

This research was supported by OGS and CINECA under the HPC-TRES program. In addition, we acknowledge the CINECA award under the ISCRA initiative, for the availability of high-performance computing resources and support (IscraC IsC83_GPSIT-2).

References

FReDNet DC; 2016: Friuli Regional Deformation Network Data Center. Istituto Nazionale di Oceanografia e Geofisica Sperimentale - OGS, Dataset, doi:10.6092/frednet.

Herring, T.A. and King, R., Floyd, M.A. and McClusky, S. C.; 2018: GAMIT Reference Manual: GPS Analysis at MIT, Release 10.7. Department of Earth. Tech. rep., Massachusetts Institute of Technology, Cambridge, Mass. URL: <http://geoweb.mit.edu/gg/Intro_GG.pdf>

Tunini, L., Magrin, A., Rossi, G., and Zuliani, D.; 2023: GNSS time series and velocities about a slow convergent margin processed on HPC clusters: products and robustness evaluation, Earth Syst. Sci. Data Discuss. [preprint], https://doi.org/10.5194/essd-2023-131, in review.

Zuliani, D., Fabris, P., Rossi, G.; 2019: FReDNet: Evolution of permanent GNSS receiver system. In: New Advanced GNSS and 3D Spatial Techniques Applications to Civil and Environmental Engineering, Geophysics, Architecture, Archeology and Cultural Heritage, Lecture Notes in Geoinformation and Cartography; Cefalo, R., Zielinski, J., Barbarella, M., Eds.; Springer: Cham, Switzerland, pp.123–137.

Lavinia Tunini, ltunini@ogs.it

Exploring Mantle Dynamics of the Cascadia Subduction System through Anisotropic Tomography with Transdimensional Inference Methods

Brandon P. VanderBeek[1], Gianmarco Del Piccolo[1], Manuele Faccenda[1]

[1]Dipartimento di Geoscienze, Università degli Studi di Padova, Padova, Italia

The Cascadia subduction system is an ideal location to investigate the nature of mantle flow and associated driving forces at a convergent margin owing to the dense network of on- and off-shore seismic instrumentation. While numerous shear wave splitting and tomography studies have been performed with these data, they have produced conflicting views of mantle dynamics collectively referred to as the Cascadia Paradox. On the overriding plate, splitting observations are consistent with large-scale 3D toroidal flow while off-shore splitting patterns are more easily explained by 2D plate-driven flow. Either geometry is difficult to reconcile with seismic tomographic models that image a fragmented Juan de Fuca slab descending beneath the Western USA. However, these observations offer only an incomplete image of Cascadia mantle structure. Shear wave splitting provides a depth integrated view of anisotropic fabrics making inferences regarding the 3D nature of mantle deformation difficult. Prior high-resolution body wave tomography typically neglects anisotropic effects which can in turn yield significant isotropic imaging artefacts that complicate model interpretation. To overcome these limitations, we invert P-wave delay times for a 3D hexagonally anisotropic model with arbitrarily oriented symmetry axes using the reversible jump Markov chain Monte Carlo algorithm. This stochastic imaging approach is particularly well-suited to the highly non-linear and under-determined nature of the anisotropic seismic tomography problem. The resulting ensemble of solutions allows us to rigorously assess model parameter uncertainties and trade-off between isotropic and anisotropic heterogeneity. We investigate whether the fragmented nature of the subducted Juan de Fuca slab is a well-resolved feature and to what extent its geometry trades off with anisotropic parameters. In light of our new 3D anisotropic model, we re-evaluate the Cascadia Paradox and attempt to reconcile disparate views of Western USA mantle dynamics.

Corresponding author: brandonpaul.vanderbeek@unipd.it